PLASMA OBSERVATIONS AT THE EARTH'S MAGNETIC EQUATOR

R. C. Olsen
Department of Physics
The University of Alabama in Huntsville
Huntsville, AL 35899

S. D. Shawhan*
600 Independence Ave., SW
NASA/HQ/EES
Washington, D.C., 20546

D. L. Gallagher, J. L. Green**, and C. R. Chappell
Magnetospheric Physics Branch
Space Science Laboratory
NASA/Marshall Space Flight Center
Huntsville, AL 35812

R.R. Anderson
Department of Physics and Astronomy
University of Iowa
Iowa City, IA 52242

October 1985

Submitted to the
Journal of Geophysical Research

* On leave from the University of Iowa
** now at NSSDC, Greenbelt, Md 20771

ABSTRACT

The magnetic equator provides a unique location for thermal plasma and plasma wave measurements. Plasma populations are found to be confined within a few degrees latitude of the equator, particularly the ions. The equatorially trapped ion population is found to be primarily hydrogen, and we find little evidence for preferential heating of heavier ions. Helium is occasionally found to be heated along with the protons, and forms about 10% of the equatorially trapped populations at such times, similar to the percentage of He+ in the cold, core plasma of the plasmasphere. One case of a heated O+ component was found, at the 0.1 % level it generally comprises in the outer plasmasphere core plasma. The heated H+ ions can be characterized by a bi-Maxwellian with kT = 0.5 to 1.0 eV, and a kT = 10-50 eV, with a density of 10-100 cm^{-3}. The total plasma density, as inferred from the plasma wave instruments measurements of the upper hybrid resonance (UHR), is relatively constant with latitude, occasionally showing a local minimum at the magnetic equator, even though the ion flux has increased substantially. The first measurements of the equatorially trapped plasma and coincident UHR measurements show that the trapped plasma is a feature of the plasmapause region, found at total plasma densities of 20-200 cm^{-3}. The warm, trapped, plasma is found in conjunction with equatorial noise, a plasma wave feature found at frequencies near 100 Hz, with a broad spectrum generally found between the proton gyrofrequency at the low frequency edge and the geometric mean gyrofrequency at the high frequency edge. This latter frequency is generally the lower hybrid resonance (LHR) for a proton- electron plasma. Sharp spatial boundaries are occasionally found with latitude, delimiting the equatorially trapped plasma. In such cases,

the equator is a region with a relative minimum in density, and it appears that field-aligned ions found at higher latitudes are 'bounced' from these boundaries, indicating a positive plasma potential of a volt or two in the equatorial region.

INTRODUCTION

Plasma and wave characteristics at the magnetic equator are important to our understanding of the magnetosphere. A number of wave-particle interactions seem to be localized at or near the equator.

GEOS 1 and 2 observations published by Young et al [1981] and Roux et al [1982] showed evidence of ion cyclotron waves and heated plasma, with a strong dependence inferred from the mass composition of the cold ion population. In particular, they found that relatively high He+/H+ ratios (0.1 to 0.5) were required to obtain wave activity, that the observed wave frequencies were strongly ordered by the helium gyrofrequency, and that helium was the ion which was primarily heated. Mauk [1982] has studied these processes from the perspective provided by ATS-6 particle and magnetometer data. The complementary case of electron heating due to electron gyroharmonics has been shown using GEOS data by Wrenn et al [1979] and Gough et al [1979].

Olsen [1981] showed ion and wave data from the SCATHA satellite between 5.5 and 6.6 RE at the magnetic equator, and inferred that a cold isotropic background or a cold field-aligned population ($E \leq 5eV$) was being heated transverse to the magnetic field line up to energies of hundreds of electron volts, with the peak ion flux typically between 50 and 100 eV. Corresponding increases in the electric field amplitudes to between 0.1 and 1.0 millivolts per meter in the 20-200 Hz frequency range were also found. Electron heating was also inferred at the equator, in agreement with the observations by Wrenn et al [1979]. Quinn and Johnson [1982] used mass spectrometer data from SCATHA to show that the ion composition of the equatorially trapped plasma population was

primarily hydrogen above 100 eV, and inferred from the distribution functions that the bulk of the ions below 100 eV were also hydrogen. The 20-200 Hz wave population associated with the heated plasma was identified as "equatorial noise", first reported by Russell et al [1970] using magnetometer measurements in the 10- to 100-Hz frequency range. These OGO-3 magnetometer measurements and wideband wave data from the Hawkeye and IMP-6 satellites [Gurnett, 1976] show that the equatorial noise spectrum has a fine structure at or near harmonics of the proton gyrofrequency, with indications of further structure at the helium and oxygen gyrofrequencies. It appears that the equatorial noise is a generalized ion Bernstein mode with the magnetic component of the wave parallel to the quasi-static magnetic field (i.e. compressional in B) and the electric component perpendicular to B [Fredericks, 1968; Gurnett, 1976]. Rauch and Roux [1982] have performed ray tracing calculations which show that this wave mode propagates radially outward. Perraut et al [1982] show GEOS observations of these waves, and link them to proton 'ring' distributions. These are ring current distributions with local minima between 1 and 10 keV, due to magnetospheric convection, and local maxima at 20-40 keV.

The purpose of this paper is to show new observations of particle and wave data from the magnetic equator from the Dynamics Explorer-1 (DE-1) spacecraft. The polar orbit of DE-1 provides a unique perspective on these equatorial phenomena. Orbital trajectories during the spring of 1982 were at nearly constant L - values across the magnetic equator These orbits result in clear latitudinal profiles of the plasma and wave characteristics, without the local time and radial variations of previous satellites. The new measurements demonstrate that the equatorial plasma

population is predominantly hydrogen and that the enhanced ion fluxes observed at the equator occur without an increases in the total plasma density. Total plasma densities for these populations are given for the first time.

INSTRUMENTATION

DE-1 was launched on August 3, 1981 into an elliptical polar orbit with apogee at 4.7 RE, It spins with a 6-s period, with its spin axis perpendicular to the orbit plane of the satellite. The orbital period is approximately 7.5 hours. Data for this study are taken from the Retarding Ion Mass Spectrometer (RIMS) and the Plasma Wave Instrument (PWI) [Chappell et al., 1981; Shawhan et al., 1981].

The RIMS consists of a retarding potential analyzer (RPA) followed by an ion mass spectrometer (IMS). The RPA voltage sweeps from 0 to 50 V, providing energy analysis, while the IMS distinguishes masses between 1 and 32 amu. For the events studied, the primary mode of the RIMS instrument is one which selects masses 1, 4, and 16 (H+, He+, and O+). There are three detector assemblies available, one looking normal to the spin axis, with the other two looking parallel and anti-parallel to the spin axis. Pitch angle distributions of the 0-50 eV ion flux are obtained from the detector looking radially outwards from the spacecraft, normal to the spin axis. This detector has an angular resolution of approximately 20° in the spin plane, and 110° perpendicular to the spin plane. The RPA on the radial detector failed prior to the period used for this study, so no energy analysis is obtained from this detector. The spin axis detectors provide RPA analysis for ions moving parallel to the spin axis. These

detectors are nominally looking perpendicular to the magnetic field at all times, with an angular resolution of 110°. One RPA/IMS cycle requires ½ second, and an angular distribution can be acquired in one spin of the satellite, i.e. in 6 seconds.

The PWI provides calibrated wave amplitude measurements from 1.8 Hz up to 409 kHz, using a low frequency correlator (LFC) from 1.8-100 Hz, and step frequency receivers (SFR) from 104 Hz to 409 kHz. The LFC covers the 1.8-100 Hz frequency range in 8 logarithmic frequency steps, and the SFR covers the remaining range in 128 steps. A complete frequency sweep requires 32 seconds - just over 5 spins of the spacecraft. The receivers may be connected to the long electric antenna (Ex), which is 200 m tip-to-tip, to the magnetic loop and search coil (B), and occasionally to the 'short' spin axis antenna 9 m tip-to-tip.

Day 86

The first example of equatorial plasma and wave measurements comes from March 27, 1982 (Day 86). As in most of the examples shown in this paper, the magnetic activity was low at this time, with Kp = 1. The satellite orbit is illustrated in Figure 1. The orbit has been projected onta a plane at 22 MLT. DE-1 is moving from south to north, beginning at L = 4 at 1730 UT. DE-1 crossed the magnetic equator at L = 4 at 1827 UT, and reached L = 5.2 at 1930 UT. The satellite is in the outer plasmasphere, or plasmapause region, throughout this period. The PWI data, described below, show the density ranging from 25 to 70 cm^{-3}.

The RIMS data are illustrated in Plate 1. Hydrogen data are displayed in the two top panels of the figure. The top panel is an RPA-time spectrogram for the (+Z) end head (90° pitch angle) data. The second panel is a spin-time spectrogram for the data taken by the radial detector at 0 V retarding potential. The center line is the ram direction which is nearly zero degrees pitch angle. The minimum pitch angle (near 0°) is indicated by the dashed white line running along the center of the spectrogram. The short-dashed line near the bottom of the panel indicates the spin phase for maximum pitch angle (nearly 180°). The fluxes are color coded, with dark blue representing low fluxes (10^5 ions/cm^2 ster s) and red represents high fluxes (10^7 ions/cm^2 ster s). The color bar on the left hand side of the figure shows this scale. Note that each of the spectrograms in this article has been scaled to emphasize the desired features, and the flux scale varies from figure to figure. The equatorially trapped plasma appears as the red regions in both panels. High fluxes, extending above 10 V on the RPA scale, and a flux peak at 90° pitch

angle in the spin-time plot identify the warm anisotropic plasma trapped at the magnetic equator. Prior to this time, the plasma is a 'ram' plasma, that is, primarily isotropic, and ordered by the spin phase (satellite velocity vector) instead of the pitch angle (magnetic field direction). After 1900 UT, faint traces of field-aligned ions become apparent, particularly in the helium (not shown). The presence of field-aligned ions indicates the satellite is leaving the plasmasphere, edging into the plasmasheet at L = 5.

The plasma wave data are shown in the bottom panel of Plate 1. The electric component of the plasma waves, from the long (Ex) antenna, show many of the features previously reported from this region of space. The Upper Hybrid Resonance (UHR), used for plasma density determinations, begins near 100 kHz at 1730 UT, and drops slowly to 45 kHz at 1930 UT. It shows enhanced signal strength 5° to 10° from the equator, but drops in intensity at the equator. This latter effect is anomalous in the DE data set; normally the UHR intensifies at the equator. Below the UHR are the electron cyclotron frequency (f_{ce}), and the first harmonic, plotted as dashed white lines. At the equator (1827 UT), the 3/2 electron gyroharmonic emission appears, as is generally found at the equator in the DE-1 data set. This is presumably the same intense emission studied by Kurth et al [1979]. At frequencies below a kilohertz the geometric mean gyrofrequency [$(f_{ci}f_{ce})^{\frac{1}{2}}$] is plotted. It drops from 500 to 200 Hz over this time period. The geometric mean gyrofrequency (f_{gmg}) is essentially equal to the proton-electron Lower Hybrid Resonance (LHR) for the regions shown in this paper, and this line is therefore labeled as the LHR [Stix, 1962]. This estimate excludes the effects of heavier ions on the LHR, i.e. a lowering of the frequency. This exclusion should generally

be a small effect in our data - a typical 10% helium component will only lower the LHR by 5%. The intense signal (red spot) below the LHR, at the equator, is the equatorial noise. Below this signal is the hydrogen gyrofrequency, plotted as a dotted white line, which remains near 10 Hz across the plot. The red band below the hydrogen gyrofrequency is primarily due to solar array noise.

Figure 2 shows the variation in the total plasma density (UHR), and the density and temperature moments for the observed hydrogen distributions. The total density drops through this period, showing a small increase at the equator. This increase is a result of following the peak in the spectra of the UHR, rather than the lower cutoff, and hence these values may be higher than the actual density. The lack of evidence for a substantial density increase at the equator provides an answer to one question raised by previous measurements. Though the equatorially trapped plasma represents a tremendous increase in flux for particle detectors, it is not primarily an increase in the total plasma density. The RPA data from the end head (90° pitch angle) were converted to distribution functions (Figure 4, described below), and then integrated to obtain the first and third moments, i.e. density and kinetic temperature. This procedure allows us to characterize the equatorially trapped plasma, even though it does not show a Maxwellian distribution. Because of the positive spacecraft potential found in such regions (+1 to +4 V on the end head), the cold background plasma is not measured by this detector. The density and temperature obtained from the end head data are therefore the parameters for the warm component only. These are the parameters plotted below the total density in Figure 2. Note that both the density and temperature of the warm plasma peak at the equator. Next, the

electric field strength near the spectral peak of the equatorial noise (167 Hz) is plotted to provide a measure of the equatorial noise intensity. Fluctuation in the electric field anplitude is due to spin modulation and beating between the spin period and sampling period.

Figure 3 shows the spin curves for hydrogen and helium prior to (3a) and at the equator crossing (3b). The off-equator data are fitted with a rammed, isotropic Maxwellian distribution, using an algorithm developed by Comfort et al [1985] Discrepancies between the model spin curves and the data indicate the beginnings of the development of anisotropic distributions. In particular, the shapes of these curves are consistent with a heat flux away from the equator [Biddle et al., 1985]. At the equator, both species exhibit trapped signatures, i.e. peaks at 90° pitch angle. The hydrogen flux is two orders of magnitude higher than the helium flux. The hydrogen spin curve has been traced and superimposed on the He+ data. The hydrogen and helium spin curves have similar shapes, except for what appears to be a field-aligned helium flux near 0° spin phase. The shape of the H+ spin curve is that expected from a bi-Maxwellian distribution, with $kT \cong 0.5$ eV, $kT_{+} \cong 5$ eV, and a +1 to +2 V spacecraft potential. This is not the only type of plasma distribution which will produce the observed spin curve, but it is a good candidate. These data do not address the question of whether the core or the tail of the distribution is heated. The higher hydrogen flux is in contrast to the preferential heating of helium inferred from GEOS 1 and 2 observations near the equator, in association with ion cyclotron waves below the hydrogen cylcotron frequency [Young et al., 1981].

Figure 4 shows the RPA data from the end head, converted into distribution function form. Superimposed on the plot is a Maxwellian

distribution with the moments, n = 12 cm^{-3} , T = 6.7 eV for hydrogen. The helium data have a similar temperature (5 eV), and a density of 0.6 cm^{-3}. The high hydrogen to helium ratio is similar to the result obtained by Quinn and Johnson [1982] at higher energies. The hydrogen to helium ratio for the heated plasma is greater than the 10:1 ratio found by RIMS for the cold plasma away from the equator.

Figure 5 shows the electric field spectral density at the magnetic equator. Six minutes of data (and hence many spins) have been averaged, showing the equatorial noise between 100 and 200 Hz, a 3/2 fce emission feature, and the UHR. Figure 5b shows an expanded spectrum from 100-300 Hz, and shows all the measurements for the six minute interval. The fluctuations are primarily due to the spin modulation of the signal. The cutoff between 185 and 204 Hz is consistent with a 10% He+ (and 0.4 % O+) ion composition, and a resulting cold plasma lower hybrid resonance frequency of 204 Hz. The equatorial noise power flux, integrated over the bandwidth, is 10^{-11} to 10^{-10} W/m^2. The magnetic component (not shown), shows a similar spectra from 100-300 Hz, with an amplitude of $10^{-2}\gamma$.

Day 52

One of the most startling observations of trapped plasma was made on February 21, 1982 (Day 52). The magnetic activity is fairly high, with Kp = 3+. Kp fluctuated between 2 and 5 during the previous 24 hour period, and this is the most active period illustrated in this article. The satellite is in the plasmasphere, at local midnight, and is in eclipse. Because the satellite is in eclipse, the potential is less positive than it would normally be, and the core, or cold plasma measurement is enhanced [Olsen et al., 1985]. The orbit for this event is shown in Figure 6. The satellite moves from L = 3.5 to 4.3, crossing the equator at 1920 UT at L = 4. The plasmapause is encountered between 1945 and 1950 UT, at L = 4.5 to 4.6. Plate 2 summarizes the plasma and wave data. Unfortunately, the PWI was turned off for the equator crossing. The RIMS data show sharp transitions from ram, isotropic plasma to the equatorially trapped distribution at 1905 and back to isotropic plasma at 1927 UT. The peak in ion flux occurs a few minutes before the nominal equator crossing, indicating either an error in the determination of magnetic latitude of 1° to 2°, or a radial variation in the heated plasma. The helium data (not shown) reveal similar behavior, with the background and heated helium populations both at about 10% of the hydrogen density. Little or no oxygen is present, in cold or heated form.

The plasma wave data show an UHR near 100 kHz over most of this period, indicating a density near 100 cm^{-3}. The transition from equatorially trapped to isotropic plasma at 1927 occurs just after the PWI is switched on again. The latter transition corresponds to an increase in density as the satellite leaves the equator, from 80 cm^{-3} to 190 cm^{-3}.

Whatever equatorial noise signature that was present at the equator has faded by the time PWI is switched on.

Both the RIMS and PWI data show a relatively rapid fluctuation in the ion flux and UHR, respectively, prior to the equator crossing. This can be considered as primarily temporal (i.e. not a result of satellite motion), or primarily spatial (i.e. the satellite is flying through quasi-static structures). In the latter case, it may either be due to radial (L-shell), latitudinal, or local time variations in the ambient plasma structure. Our current explanation of these fluctuations and a number of similar observations, is that there is a latitudinal structure, established by a plasmasphere filling process which introduces shock fronts, and discontinuities, into the field-aligned structure. Note that this structure does not persist through the equator, as though the equator represents a barrier to inter-hemisphere communication.

Figure 7 summarizes the reduced plasma parameters for this set of observations. The difference between the electron and ion densities, derived from PWI and RIMS, respectively, can be explained by a +1 V potential on the detector. The ion density is constant through the equator, while the temperature increases by an order of magnitude. Both the ion and electron density increase sharply at the high latitude boundary to the region of heated plasma at 1927 UT. Note that the density is higher above the equator than it was at lower L-shells below the equator.

Figure 8 contrasts the spin curves prior to (a), during (b), and after (c) the equator crossing. The ram distributions are again fitted with rammed, Maxwellian plasma distributions. The hydrogen spin curves at the equator appear to be a combination of isotropic plasma and trapped plasma. In particular, the curvature near 0° spin phase indicates the

angular distribution is not so much a bi-Maxwellian (which results in curves like those in Figure 3), as the sum of a cold and warm population. The isotropic hydrogen component has a density which is less than 10% of the off-equator values. This low percentage suggests that the bulk of the cold isotropic plasma has been converted into the heated, equatorially trapped plasma, and that in this case the heated plasma is not just the heated tail of the core plasma.

RPA data from the end head are again converted into distributions functions, as shown in Figure 8, with equivalent Maxwellian distributions plotted over the data. There is little evidence of cold plasma in the 0-10 eV energy range of panel E.

Day 75

One of the implications of the previous example is that there are relatively sharp spatial (latitudinal) boundaries delimiting the region of equatorially trapped plasma, particularly in magnetic latitude. This idea is extended by the next example from March 16, 1982 (Day 75). Kp is 1, and was between 1 and 2 for the previous 24 hours. Plate 3 shows 2 orbital segments for this day. The satellite crosses the plasmapause twice over this period, first at 1402 UT, and again near 1510 UT, both times at L = 4.2, This is the 100 cm^{-3} boundary, and is quite sharp at 1400 UT ($\lambda m = -37°$). One peculiarity of the plasmapause structure found on this day is that the density shows a local maximum from 1400-1415 UT (L = 4.3 to 4.0, $\lambda m = -37°$ to $-27°$). The density maximum does not appear in the later equatorial crossing of the same L-shells. Unfortunately, there is a data gap from 1430-1500 UT. The plasma density is the same at 1500 UT as at 1430 UT, so we can only speculate that it was constant over this time period. Further information on the plasmapause location can be obtained from ISEE-1, which encounters the plasmapause (inbound) at 1740-1745 UT, 7 LT, $\lambda = -37°$, 3.1 RE, L = 5.0 to 5.5. Outbound, ISEE-1 crosses the 100 cm^{-3} boundary at 1950 UT, 22 LT, 4 RE, $\lambda = 13°$, and L = 4.3. This combination of boundary crossings bracket the DE measurements at local midnight (actually 23 LT).

Plate 4 shows the RIMS data for the equator crossing. The helium fluxes have been enhanced by two orders of magnitude to bring them onto the hydrogen flux scale. A plasmapause signature is visible near 1510 UT. In the RPA data (panels A and C), the red regions in the lower left hand corners show the fading of the cold plasmasphere plasma. In the

He+ spin-time spectrogram (panel D), evidence of field-aligned plasma appears, primarily in the 180° pitch angle (-180° spin phase) data. The hydrogen spin-time spectrogram (panel B) shows a distribution peaked at 90° pitch angle, as one now expects at the equator. Also, the hydrogen RPA data (panel A), shows a substantial increase in flux at the equator. The helium RPA data show a minimum in this region, with distinct boundaries at 1520 UT and 1535 UT ($\lambda m = \pm 3°$) as though helium ions are excluded from the equator. The intensity of the field-aligned He+ flux also decreases over this period, with a particularly noticeable increase upon leaving this region at 1537.

Plate 5 shows the PWI data for this period. The short spin axis antenna is being used at this time. The data from this antenna are noisier than those shown in the previous examples, and are only used to identify the UHR. The UHR and 3/2 f_{ce} signals intensify near the equator, and a brief signal is found just below the LHR at 1525 UT. The broad spectrum previously associated with the Bernstein modes is not seen here, and the emission below the LHR at 1525 UT may not be the "equatorial noise" normally found with the equatorially trapped plasma, but rather a lower hybrid resonance emission.

Figure 9 shows the reduced plasma parameters for this period. The format of Figure 9 is similar to that used in Figure 7. The UHR derived total electron density is plotted at the top. Much of the fluctuation following 1520 UT is probably a fluctuation between enhancements of the 6th and 7th ($n+\frac{1}{2}$) electron gyroharmonics which mask the UHR noise. Next the hydrogen and helium densities, as obtained from the RPA data, are plotted. The helium values have been multiplied by 10 to compress the plot. The hydrogen and helium densities are highest at

1500 UT, as the satellite is leaving the plasmasphere. Again the difference between the proton and electron density from 1500-1510 is primarily due to a +1 to +2 V detector potential. The warm proton density is then constant through the equator, while the helium density shows a minimum, as implied by the spectrogram. The ion density from 1520-1600 is less than the electron density because most of the core plasma is hidden by the increasingly positive detector potential [Olsen et al. 1985]. The proton temperature, plotted below the density profiles, shows an order of magnitude increase at the equator.

These data show:

a) a case where only protons are heated,

b) the thermal helium is excluded from the equatorial region, and

c) only a small wave signal near the LHR is found.

We infer that the heating of the plasma at the equator increases the plasma potential, which causes a decrease in the ion density ($\exp(-e\Phi/kT)$). This positive potential causes the field-aligned He+ flux to lose kinetic energy as it enters this region. The reduced flow velocity results in a lower flux. The latitudinal extent of the LHR related emission does not match that of the heated ions, and the power is substantially lower than that normally found in the equatorial noise. It is likely that the increase in the ion temperature is not due to the observed emissions near the LHR frequency.

The examples shown so far have illustrated the ideas that the equatorially trapped plasmas are primarily hydrogen, and that these plasmas exhibit a temperature increase, not a density increase. Indeed, the equatorial region may represent a local minimum in density. The

conversion from isotropic to equatorially trapped plasma has been shown in several cases, and indications of an apparent transition from field-aligned to trapped plasma were found in the last example. In the next case, indications of a density minimum are found, along with suggestions that the field-aligned ions are either converted into the trapped plasma at a sharp boundary, or that they are being reflected at a potential structure near the equator.

Day 126 - 1100 UT

Two orbits from May 6, 1982 (Day 126) are shown. The orbit which provided an equator crossing at 1100 UT is illustrated first, in Plate 6. The satellite crosses the plasmapause at high and then low latitudes. The high latitude crossing is at 0930 UT. The satellite is at L = 4.7, λm = -22°. As the satellite approaches the equator, it again crosses the density gradient, but at a lower L-value. The low latitude gradient is found at L = 4.6, λm = -6°. This has been interpreted as shown by the blue area in Plate 5, with a plasmasphere that is dimpled near the equator, and bulges outward between -7° and -22° magnetic latitude. The satellite is at local dusk (19.6 LT). Kp was 2-, and was between 2- and 2+ for the previous 12 hours, and was 3 for the 12 hours before that.

Plate 7 shows the RIMS and PWI data for this period. The RIMS spin-time spectrogram for hydrogen shows a field-aligned distribution which abruptly becomes a 'pancake' distribution at 1035 UT. The helium data are similar to the hydrogen, with fluxes 1 to 2 orders of magnitude lower than the hydrogen flux. The PWI data show a drop in the UHR at 1035 UT, and the appearance of the equatorial noise. There is an intensification of the UHR, the appearance of continuim radiation, and at least the first 4 of the $n+\frac{1}{2}$ electron gyroharmonic emissions at the equator.

Figure 10 shows the reduced plasma parameters for this day. The top curve shows the decrease in density from 100 cm^{-3} to 40 cm^{-3} from 1033 to 1038 UT. The density of the warm hydrogen (the core, or cold component, is again "hidden" by the positive detector potential) shows a sharp rise, reflecting the increase in the plasma temperature, as shown in the next curve of the figure. At the bottom of the figure, the 105 Hz

signal from the spin axis antenna indicates a similar abrupt transition in the equatorial noise. (The signal in this antenna is near background from 1000-1030 UT.)

Figure 11 shows the hydrogen and helium spin curves, which show the distribution associated with a bi-Maxwellian distribution found previously. Figure 12 shows the hydrogen distribution function, with a low energy component inferred from 0 to 3 eV. Figure 13 shows the electric field spectrum. Most of the wave power appears to be in the 10-100 Hz frequency range. The spectrum is again bounded by the lower hybrid frequency (or geometric mean gyrofrequency).

The sharp boundary in density and plasma characterisitics at 1035 UT ($\lambda m = -7°$), can be interpreted as a boundary in latitude, resulting from heating and a subsequent increase in plasma potential near the equator. The field-aligned ions seen before 1030 UT approach the equator from behind the satellite, "bounce" off the electrostatic potential barrier, and are then seen returning from the equator (at 0° spin phase). The (apparently) larger flux at 0° spin phase reflects the low energy of the field-aligned ions, and the effect of the satellite velocity, which must be comparable to the field-aligned flow velocity (a few km/s). As in the first example shown, there is a strong correlation between the equatorial noise and equatorially trapped plasma.

An alternative explanation for the disappearance of the field-aligned ions at the density gradient at 1035 UT is that the increase in satellite potential associated with that density decrease was sufficient to exclude the field-aligned population from the satellite. A detector potential of several volts positive is to be expected at a plasma density of 40 cm^{-3},

and the kinetic energy of such field-aligned flows can be as low as a few eV [Olsen et al. 1985].

Day 126 - Hour 3

The second of the events from May 6, 1982, provides similar plasma measurements to those shown first in this article, from March 27. The satellite moves from the plasmasphere, and a region of isotropic plasma, into the equatorially trapped distributions. This orbit also features a high latitude plasmapause crossing, and a fortuitous overlap with ISEE-1. The satellite orbits are illustrated in Figure 14. DE-1 crosses the equator at L = 4.3 at 0300 UT, 20 LT. DE-1 had crossed this L-shell earlier in the same orbit at 0128, at -42° λ_m and 20 LT. ISEE-1 is outbound from perigee at this time, crossing L = 4.3 at 0018 UT, at 24° λ_m, at 18 LT. This is nominally the plasmapause position at high latitudes, as determined by both satellites.

The DE-1 data for this orbit are summarized in Plate 8. The hydrogen data are shown in the top two panels. The RPA data are shown in the top panel (A). A plasmapause signature is found between 0120 and 0130 UT, where a warm plasma is found. The satellite enters the plasmasphere, and remains there until reaching the magnetic equator. The spin distributions show rammed, isotropic plasma from 0130 to 0230, again indicating the satellite is in the plasmasphere. The three narrow vertical stripes at 0141, 0148, and 0157 are the similar to the narrowly confined latitudinal structure inferred from the February 21 data (Plate 2). These are primarily density enhancements, not temperature increases. At the equator, the temperature increases, but the density does not. The plasma wave data show the UHR is monotonically dropping. There is not a clear equatorial noise signature on this day, but there may be a signal near the

LHR at the equator, and a lower frequency feature prior to the equator crossing. (These spectra are discussed below.)

The reduced plasma parameters for the equator segment are shown in Figure 15. The total plasma density drops monotonically over this period, while the warm ion density and temperature peak at the equator. The electric field spectra at 0242-0245 (prior to the equator crossing), and 0254-0258 (at the equator) are shown in Figure 16. The pre-equator spectrum (the bottom curve) shows the broad structure normally found at the equator, while the 0254-0258 data (top curve) show a peak which is essentially limited to one channel (185 Hz, while fgmg is 205 Hz). Neither spectra is as intense as the more typical example in Figure 13.

ISEE-1 crosses this region at nearly the same time as DE-1. The ISEE-1 data can therefore be used to determine the radial density profile for the DE-1 equator crossing. Figure 17 shows the ISEE-1 plasma wave data. The UHR comes on scale at 400 kHz at 2335 UT, and drops monontonically down to 25 kHz at 0130 UT, as the satellite moves outward. The density profile for this segment is plotted vs. "L" in Figure 18. Near L = 4.3, the density profile was fitted with the functional form: n_o (L/4.3)$^{-x}$, from L = 3.9 to 5.2. The resulting parameters were n_o = 41 cm^{-3}, x = 4.5. The density value is the same as the equatorial density observed by DE-1 at the equator. For a broader range of L (L = 3.9 to 6) the least square fit (LSF) resulted in x = 4, and a similar density. Using the $L^{-4.5}$ density profile, it is possible to eliminate the "L" dependence of the DE-1 latitude profile. When this is done, it is found that the density is constant from -30° to +10° magnetic latitude, to within the accuracy of the measurements. The result does not change if an L^{-4} profile is used.

This example demonstrates that the density remains constant while the temperature increases by an order of magnitude. The combination of ISEE and DE data also clearly shows that DE is in the region of the plasmapause density gradient while crossing the equator.

DISCUSSION

The DE-1 RIMS and PWI observations near the magnetic equator have provided a new perspective on the equatorially trapped plasma and equatoral noise. This region of enhanced temperatures, and 90° pitch angle distributions, is limited to ±5° to ±10°magnetic latitude. The narrower extent appears to be associated with higher densities.

The equatorially trapped plasmas occur in the plasmapause region, where the total densities range from 20 cm^{-3} to 200 cm^{-3}. The warm, trapped plasma, comprises 50-90% of the total, so at times the bulk of the ambient plasma is heated.

The equatorially trapped plasma is primarily composed of protons. At times, only H+ is heated. When the He+ ions are heated, the warm He+ population forms about 10% of the equatorially trapped plasma, the same ratio found in the cold plasma of the outer plasmasphere. This means there is no preferential heating of heavy ions. This is in contrast to the behavior associated with ion cyclotron waves, as observed on GEOS [Young et al, 1981]. One case of a heated 0^+ component was found, at a relative concentration of 0.1%.

The tremendous enhancments in flux encountered at the magnetic equator were initially associated with the idea of density enhancements [Olsen, 1981]. The addition of plasma wave data has shown that the equator is not generally a region of enhanced density. The enhancement in ion flux is the result of a temperature increase. There may in fact be a density

minimum at the equator. These cases are associated with sharp spatial boundaries, and the apparent reflection of low energy field-aligned ions. The density minimum may be caused by an increase in the plasma potential, caused by RF heating. Such a potential would explain the apparent reflection of ionospheric flows.

Such processes are observed to operate in laboratory plasmas, particularly in tandem drift mirror devices [Dimov et al, 1976; Coensgen et al. 1980]. Figure 19 shows a schematic version of the inferred plasma potential and plasma density variations in the magnetosphere. In a mirror device, the electrostatic potential is added in a small 'dimple' magnetic field region at the ends of the mirror, but the geometry is otherwise quite similar. The enhanced plasma potential in the laboratory devices is created by heating the plasma at the ends. This warm, trapped plasma then forms a barrier to field-aligned particles from the main section of the mirror. In our geometry, the heating is at the center of the "device".

An alternate perspective on this process is that the enhanced plasma temperatures at the equator would result in higher plasma pressures, if the ambient plasma density does not decrease. This assumes a requirement for equality in plasma pressure along the field line (in equilibrium).

The plasma waves observed at the magnetic equator, and presented in this paper, fall into two categories. The first, we term equatorial noise, which has been associated with the broad spectrum of electromagnetic waves which fill much of the frequency range between the proton gyrofrequency and the geometric mean gyrofrequency. The high frequency limit is

considered to be the lower hybrid frequency. These characteristics are consistent with the previous identification of these waves as an electromagetic Bernstein mode, as developed by Fredericks [1968] and observed by Gurnett [1976]. A second category is a narrow (1 to 3 channels wide) spectral feature just below the geometric mean gyrofrequency, tentatively identified as a lower hybrid resonance emission.

The perspective of the DE-1 plasma wave observations differs significantly from that of the recent GEOS observations, reported by Perraut et al. [1982]. Their observations were oriented towards the magnetic component in the 0-8 Hz frequency range, while the DE-1 observations are primarily of the electric component, with most of the data coming at frequencies above 100 Hz, much like the original Hawkeye and IMP-8 observations [Gurnett, 1976]. The majority of the wave power is apparently in the first few harmonics above the proton gyrofrequency, in the magnetic component, so both sets of observations need to be considered in studies of wave generation, and effects on the plasma.

The generation of the Bernstein mode has been discussed by Gul'Elmi et al [1975], Curtis and Wu [1979], and Perraut et al. [1982]. The two earlier papers suggest that the energy source is meV particles, and use relativistic terms in the wave growth calculation. Perraut et al. suggest that the energy source is the 1-10 keV ion portion of the ring current. They use a spectral feature of the ion distribution function termed the "deep proton minimum" [DeForest and McIlwain, 1971]. This is a minimum in the ion distribution function at all pitch angles resulting from the boundary in energy between eastward and westward convecting ring

current ions. A ring current energy source is consistent with IMP-8 observations of a strong DST correlation for the equatorial noise [T. L. Aggson, private communication, 1983].

The resultant heating of the thermal ions by the equatorial noise has been discussed by Curtis [1985]. He invokes stochastic processes to explain the heating, based on the inferences from the original SCATHA electrostatic analyzer observations [Olsen, 1981]. Additional work in this area needs to recognize the new information that the bulk of the plasma is heated, not just the tail of the distribution.

Some perspective on these observations can be obtained by considering the energy densities in each of the pertinent particle populations, and the observed waves.

a) Ring current - 10 keV, 1 cm^{-3}, 10^{-9} J/m^3;

b) Thermal plasma - 10 eV, 10 cm^{-3}, 10^{-11} J/m^3;

c) Cold plasma - 1 eV, 90 cm^{-3}, 10^{-11} J/m^3;

d) waves - electric - 10^{-4} V/m, 10^{-19} J/m^3;

magnetic - 10^{-2} γ, 10^{-16} J/m^3.

There is substantially more power in the nominal energy source, and in the heated plasma, than in the waves.

The relatively high energy density in the 'heated' plasma does not preclude the observed waves from being the energy source for these ions. It is possible that these waves represent a highly efficient conduit for the transfer of energy from the ring current to the plasmasphere. If we assume that the waves propagate radially and are limited to ±10° latitude, an estimate of the necessary time to heat the cold plasma can be made. Since the Bernstein mode has stop bands at each gyroharmonic, it is limited in the radial distance it can propagate. Using this limit, and the observed energy densities, an estimate of one hour results for the time needed to heat the ambient plasma.

Our view of these data is summarized in Figure 20. Field-aligned flows from the ionosphere fill the outer plasmasphere, and are thermalized by 'shock' processes both along the field line, and at the equator, as suggested by the original polar wind theory of Banks and Holzer [1968]. In this context, the creation of the equatorially trapped plasma may be an element

of the plasmasphere filling process. The two hemispheres are seperated by the plasmas and potential structure at the equator. It is possible that the filling process begins off the equator, resulting in a region of relative minimum density at the equator which presists through the filling process. The greater latitudinal range of the heated plasma region at the plasmapause is inferred from observations on DE-1, but was initially suggested by T. L. Aggson [private communications, 1983].

In retrospect, we have been fortunate that the plasmapause was found so regularly at $L \leq 4.5$. A different apogee could have resulted in a much more limited data set. The combination of ISEE and DE data helped substantially in resolving the "L" vs "λm" parameters. The next major improvement in our understanding probably depends on the information obtainable from an equatorial ($\lambda m \leq 3°$) satellite which produces radial profiles, such as the Explorer 45 satellite, or the proposed ISTP Equator satellite.

ACKNOWLEDGEMENTS

We thank A. P. Biddle for recognizing, and explaining, the relevance of the tandem mirror to our observations. We would like to thank the programming staffs of Boeing Corp. and Intergraph Corp., particularly Dick West.

Our thanks to the Data Systems Technology Program and the SPAN network for providing the computer resources to analyze the data.

This work was supported by NAS8-33982 and NSFATM8-300426 at UAH, and NAS_____at the University of Iowa.

BIBLIOGRAPHY

Banks, P. M., and T. E. Holzer, The polar wind, J. Geophys. Res., 73, 6846, 1968.

Biddle, A. P., T. E. Moore, and C. R. Chappell, Evidence for ion heat flux in the light ion polar wind, J. Geophys. Res., 90, 8552-8558, 1985.

Chappell, C. R., S. A. Fields, C. R. Baugher, J. H. Hoffman, W. B. Hanson, W. W. Wright, and H. D. Hammack, The retarding ion mass spectrometer on Dynamics Explorer A, Space Sci. Inst., 5, 477-491, 1981.

Coensgen, F. H., C. A. Anderson, T. A. Casper, J. F. Clauser, W. C. Condit, D. L. Correll, W. F. Cummins, J. C. Davis, R. P. Drake, J. H. Foote, A. H. Futch, R. K. Goodman, D. P. Grubb, G. A. Hallock, R. S. Hornady, A. L. Hunt, B. G. Logan, R. H. Munger, W. E. Nexsen, T. C. Simonen, D. R. Slaughter, B. W. Stallard, and O. T. Strand, Electrostatic plasma-confinement experiments in a tandem mirror system, Phys. Rev. Lett., 44, 1132-1135, 1980

Curtis, S. A., Equatorial trapped plasmasphere ion distributions and transverse stochastic acceleration, J. Geophys. Res., 90, 1765-1770, 1985.

Curtis, S. A., and C. S. Wu, Gyroharmonic emissions induced by energetic ions in the equatorial plasmasphere, J. Geophys. Res., 84, 2597-2607, 1979.

DeForest, S. E., and C. E. McIlwain, Plasma clouds in the magnetosphere, J. Geophys. Res., 76, 3587-3611, 1971.

Dimov, G. I., V. V. Zakaidakov, and M. E. Kishinevsky, Thermonuclear confinement system with twin mirror systems, Sov. J. Plasma Phys., 2, 326-333, 1976.

Fredericks, R. W., Structure of generalized ion Bernstein modes from the full electromagnetic dispersion relation, J. Plasma Phys., 2, 365-380, 1968.

Gough, M. P., P. J. Christiansen, G. Martelli, and E. J. Gershuny, Interaction of electrostatic waves with warm electrons at the geomagnetic equator, Nature, 279, 515-517, 1979.

Gul'Elmi, A. V., B. I. Klaine, and A. S. Potapov, Excitation of magnetosonic waves with discrete spectrum in the equatorial vicinity of the plasmapause, Planet. Space Sci., 23, 279-286, 1975.

Gurnett, D. A., Plasma wave interactions with energetic ions near the magnetic equator, J. Geophys. Res., 81, 2765-2770, 1976.

Kurth, W. S., J. D. Craven, L. A. Frank, and D. A. Gurnett, Intense electrostatic waves near the upper hybrid resonance frequency, J. Geophys. Res., 84, 4145-4164, 1979.

Mauk, B., Electromagnetic wave energization of heavy ions by the electric "phase bunching" process, Geophys. Res. Lett., 9, 1163-1166, 1982.

Olsen, R. C., Equatorially trapped plasma populations, J. Geophys. Res., 86, 11235-11245, 1981.

Olsen, R. C., C. R. Chappell, J. L. Green, D. L. Gallagher, D. A. Gurnett, The hidden ion population - revisited, J. Geophys. Res., in press, 1985.

Perraut, S., A. Roux, P. Robert, R. Gendrin, J.-A. Sauvaud, J.-M. Bosqued, G. Kremser, and A. Korth, A systematic study of ULF waves above F_H^+ from GEOS-1 and -2 measurements and their relationships with proton ring distributions, J. Geophys. Res., 87, 6219-6236, 1982.

Quinn, J. M., and R. G. Johnson, Composition measurements of warm equatorially trapped ions near geosynchronous orbit, Geophys. Res. Lett., 9, 777-780, 1982.

Rauch, J. L., and A. Roux, Ray tracing of ultra low frequency waves in a multicomponent plasma. Consequences on the generation mechanism of ion cyclotron waves, J. Geophys. Res., 87, 8191-8198, 1982.

Roux, A., S. Perraut, J. L. Rauch, C. de Villedary, G. Kremser, A. Korth, and D. T. Young, Wave particle interactions near Ω_{He^+} onboard GEOS 1 and 2. 2. Generation of ion cyclotron waves and heating of He+ ions, J. Geophys. Res., 87, 8174-8190, 1982.

Russell, C. T., R. E. Holzer, and E. J. Smith, OGO 3 observations of ELF noise in the magnetosphere, 2. The nature of the equatorial noise, J. Geophys. Res., 75, 755-768, 1970.

Shawhan, S. D., D. A. Gurnett, D. L. Odem, R. A. Helliwell, and C. G. Park, The plasma wave and quasi-static electric field experiment (PWI) for Dynamics Explorer A, Space Sci. Inst., 5, 535-550, 1981.

Stix, T. H., The theory of plasma waves, published by McGraw-Hill Book Company, Inc., New York, 1962.

Wrenn, G. L., J. F. E. Johnson, and J. J. Sojka, Stable "pancake" distributions of low energy electrons in the plasma trough, Nature, 279, 512-514, 1979.

Young D. T., S. Perraut, A. Roux, C. de Villedary, R. Gendrin, A. Korth, G. Kremser, and D. Jones, Wave-particle interactions near Ω_{He^+} observed on GEOS 1 and 2. 1. Propagation of ion cyclotron waves in He+-rich plasma, J. Geophys. Res., 86, 6755-6772, 1981.

Plate 1. A) RPA-time spectrogram for H+ measurements in the +Z (α = 90°) detector. B) Spin-Time spectrogram for H+, taken at 0V RPA. This detector responds to H+ ions from 0 eV to several hundred eV. C) Plasma wave data from the long electric antenna, perpendicular to the spin axis.

Plate 2. A) RPA-time spectrogram for H+ (α = 90°). B)Spin time spectrogram for H+. C) Plasma wave data from the long electric antenna.

Plate 3. Orbit plot for March 16, 1982. The plasmasphere is shown in green, the plasmapause region in blue. The region of equatorially trapped plamsa is in red.

Plate 4. A) RPA-time spectrogram for H+. B) Spin-time spectrogram for H+. C) RPA-time spectrogram for He+. D) Spin-Time spectrogram for He+.

Plate 5. Plasma wave data from the spin axis electric field antenna. Raw telemetry ranges from 0-256, with only the bottom half of that range used for this plot. The telemetry is the uncalibrated, logarithmically compressed antenna voltage.

Plate 6. Orbit plot for May 6, 1982. The plasmasphere is in blue, the equatorially trapped plasma region is in red.

Plate 7. A) Spin-time spectrogram for H+. B) Plasma wave data from the long electric antenna.

Plate 8. A) RPA-time spectrogram for H+. B) Spin-time spectrogram for H+. C) Plasma wave data from the long electric antenna.

Figure 1. Orbit plot for March 27, 1982 (day 86) in solar magnetic coordinates. The orbit has been rotated into a common plane at the local time of 2230.

Figure 2. Summary of plasma parameters. Total electron density, dervived from PWI, is at the top. The ion distribution function is integrated to obtain the ion (H+) density and temperature. Since the plasma is assumed to be isotropic when the distribution function is calculated, and integrated, the first moment is a pseudo-density, denoted $4\pi\partial n/\partial\Omega$ in these plots. The electric field strenght at 167 Hz is next. The magnetic latitude (λm) and McIlwain "L" parameter are at the bottom, with scales on the left hand and right hand sides, respectively.

Figure 3. A)Spin curves for H+, He+, and O+ prior to the equator crossing. The data were fitted with the curves shown, and the resulting plasma parameters are noted beside each curve. B) Spin curves for H+ and He+ at the magnetic equator. The line drawn through the He+ data is the trace of the H+ curve.

Figure 4. Ion distribution functions for H+. A) Prior to the equator crossing. B) At the equator.

Figure 5. Electric field spectrum at the equator. The dotted patern in A is the noise level.

Figure 6. Orbit plot for February 21, 1982.

Figure 7. Summary of plasma parameters with total electron density (e), ion (H+) density (i), ion (H+) temperature (T), and magnetic latitude and L.

Figure 8. A) Spin curves for H+ (.) and He+ (4) prior to the equator crossing, with fits. B) Spin curves at the equator, with lines drawn for the same temeperatures found in A and C, at reduced densities. C) Spin curves after the equator crossing. D) H+ distribution function for the period shown in A. E) H+ distribution function for the period shown in B. Note the change in energy scale as compared to panels D and F. F) H+ distribution function for the period shown in C.

Figure 9. Summary plot for March 16, 1982. Total electron density, hydrogen density, helium density (x10), hydrogen temperature, magnetic latitude and L.

Figure 10. Summary plot for May 6, 1982, 10:00 to 11:30 UT.

Figure 11. Spin curves for hydrogen and helium at the magnetic equator.

Figure 12. H+ distribution function at the magnetic equator.

Figure 13. Electric field spectrum at the magnetic equator.

Figure 14. Orbit plot for DE-1 and ISEE-1.

Figure 15. Summary plot for May 6, 1982.

Figure 16. Electric field frequency spectrum, May 6, 1982.

Figure 17. ISEE-1 frequency time spectrogram, May 5-6, 1982.

Figure 18. ISEE-1 density profile, on a log-log scale. Least square fits (LSF) are done for two seqments.

Figure 19. Tandem mirror configuration as postulated for the magnetosphere. The small bump in potential at the equator (of order 1 volt) is sufficient to reduce the ambient plasma density, and "bounce" low-energy field-aligned flows.

Figure 20. Summary figure for the equatorial heating processes inferred from the observations in ths paper.

DYNAMICS EXPLORER I
MARCH 27, 1982
RETARDING ION MASS SPECTROMETER

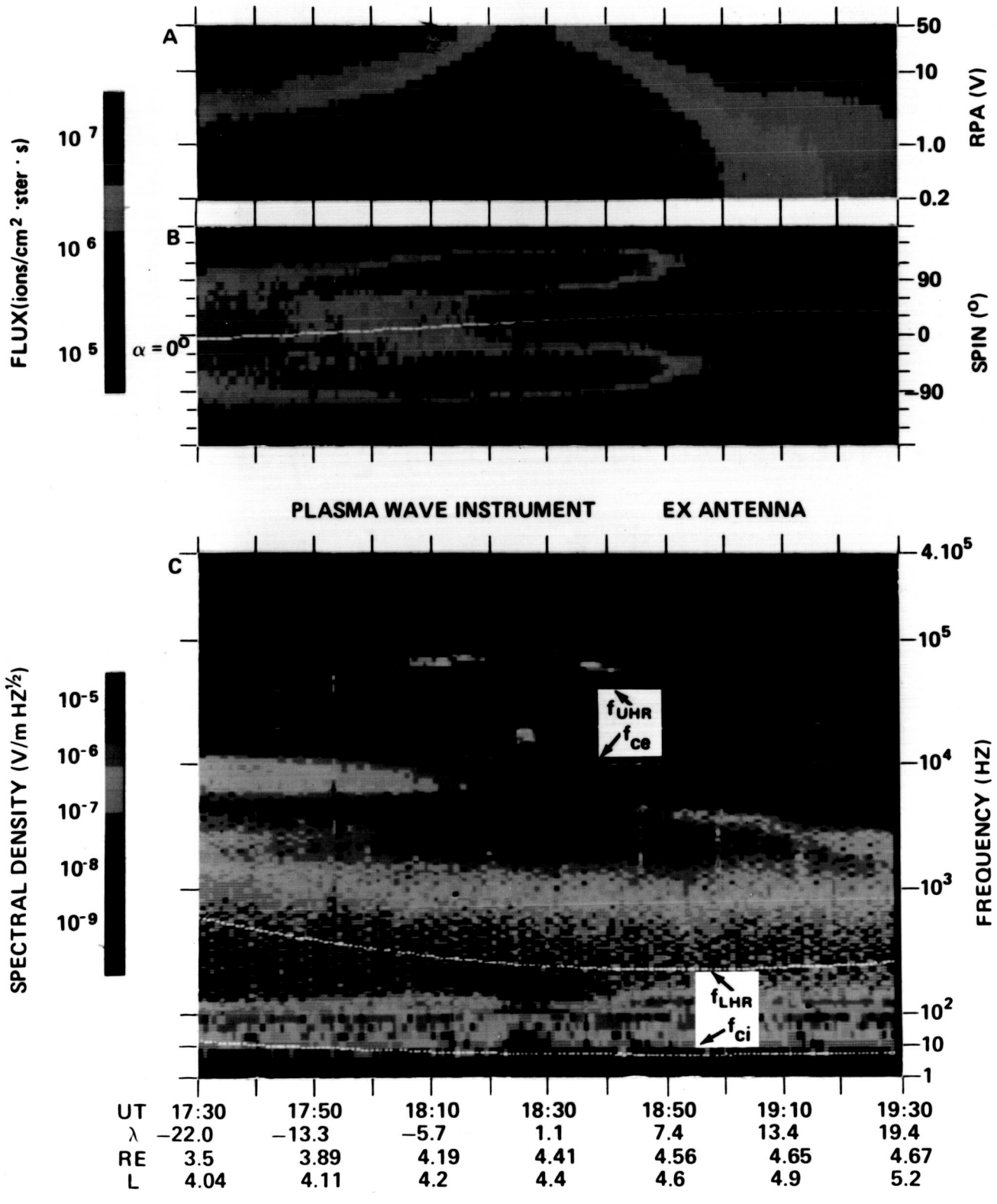

DAY 86

Plate 1

DYNAMICS EXPLORER I
FEBRUARY 21, 1982

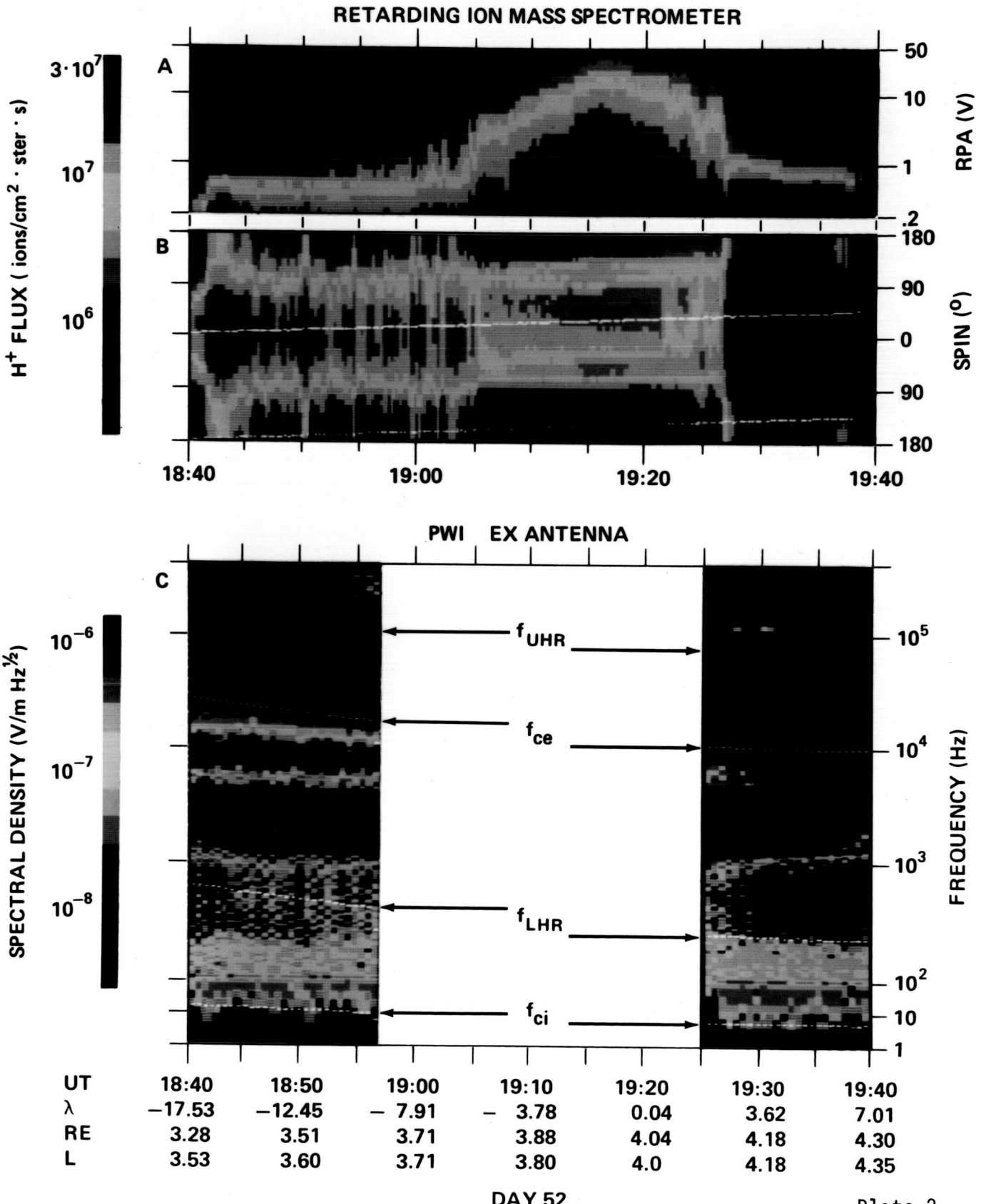

UT	18:40	18:50	19:00	19:10	19:20	19:30	19:40
λ	−17.53	−12.45	− 7.91	− 3.78	0.04	3.62	7.01
RE	3.28	3.51	3.71	3.88	4.04	4.18	4.30
L	3.53	3.60	3.71	3.80	4.0	4.18	4.35

DAY 52

Plate 2

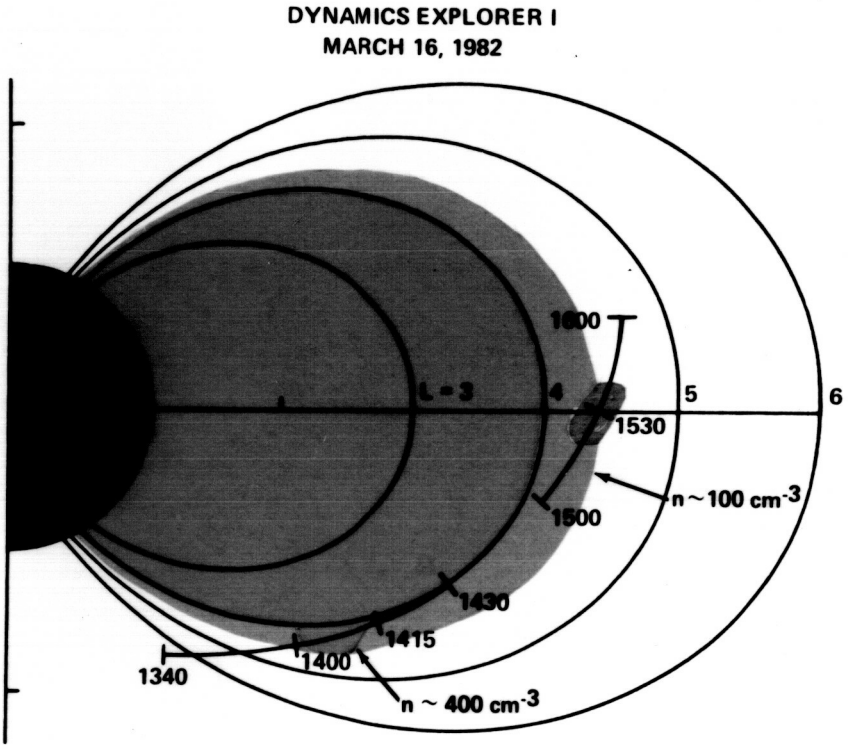
DYNAMICS EXPLORER I
MARCH 16, 1982
1600
L = 3
4
5
6
1530
n ~ 100 cm-3
1500
1430
1415
1400
1340
n ~ 400 cm-3
DAY 75

Plate 3

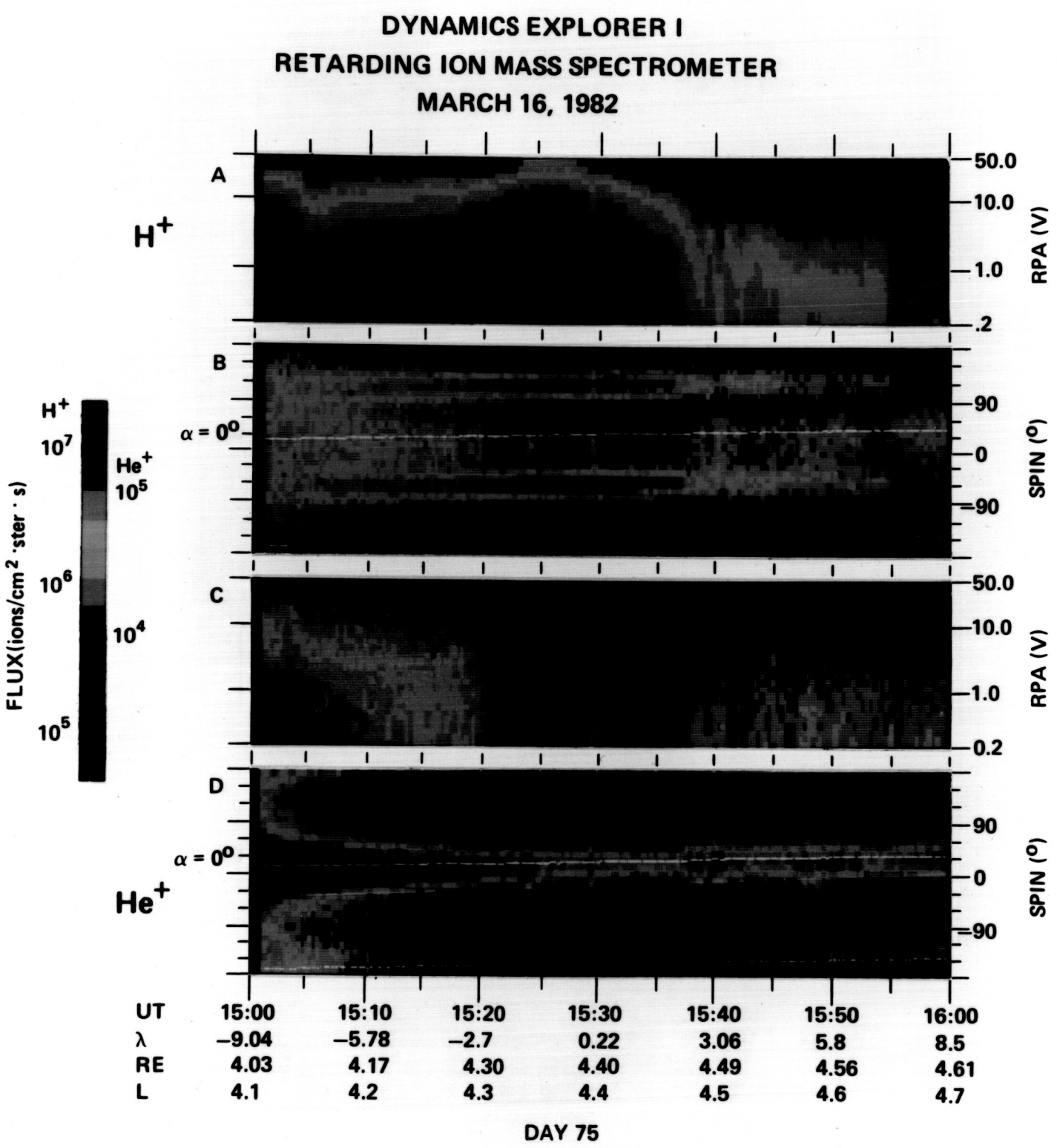
DYNAMICS EXPLORER I
RETARDING ION MASS SPECTROMETER
MARCH 16, 1982
A
H+
50.0
10.0
1.0
.2
RPA (V)
B
α = 0°
90
0
-90
SPIN (°)
H+
10^7
He+
10^5
10^6
10^4
10^5
FLUX(ions/cm^2 ·ster · s)
C
50.0
10.0
1.0
0.2
RPA (V)
D
α = 0°
He+
90
0
-90
SPIN (°)
UT 15:00 15:10 15:20 15:30 15:40 15:50 16:00
λ -9.04 -5.78 -2.7 0.22 3.06 5.8 8.5
RE 4.03 4.17 4.30 4.40 4.49 4.56 4.61
L 4.1 4.2 4.3 4.4 4.5 4.6 4.7
DAY 75

Plate 4

DYNAMICS EXPLORER I

PLASMA WAVE INSTRUMENT

MARCH 16, 1982

EZ ANTENNA

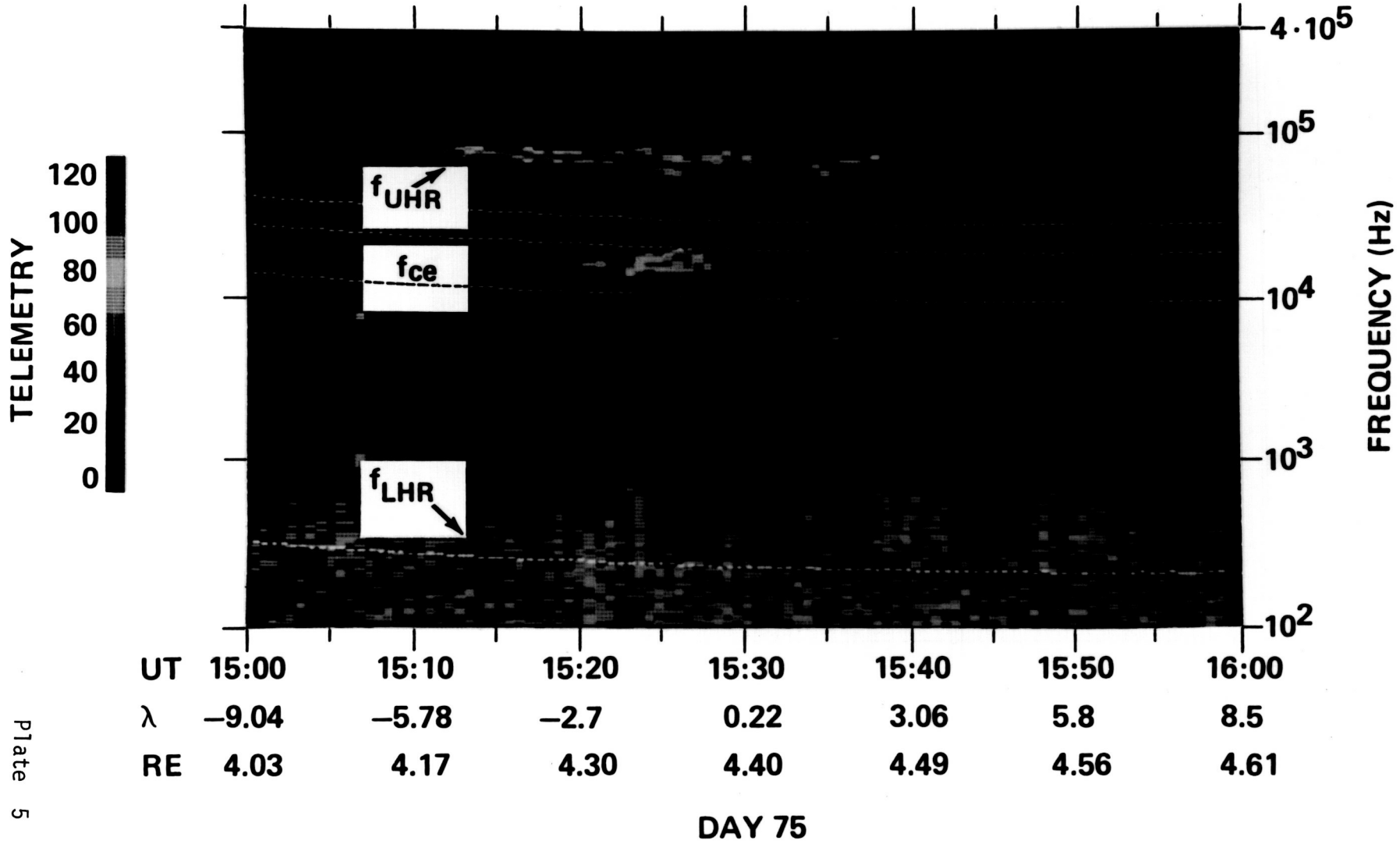

Plate 5

DYNAMICS EXPLORER I
MAY 6, 1982

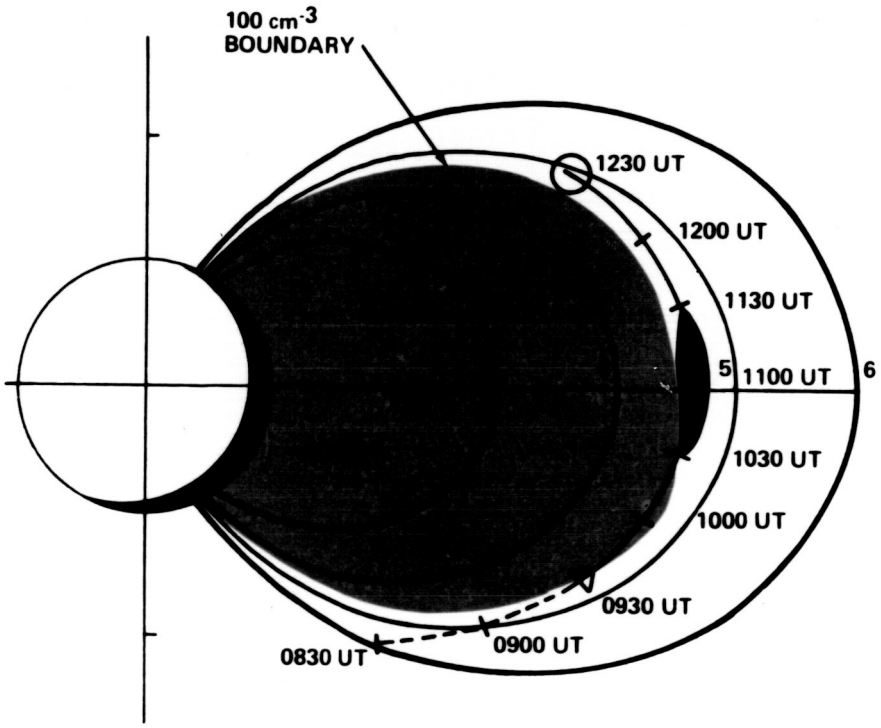

DAY 126

Plate 6

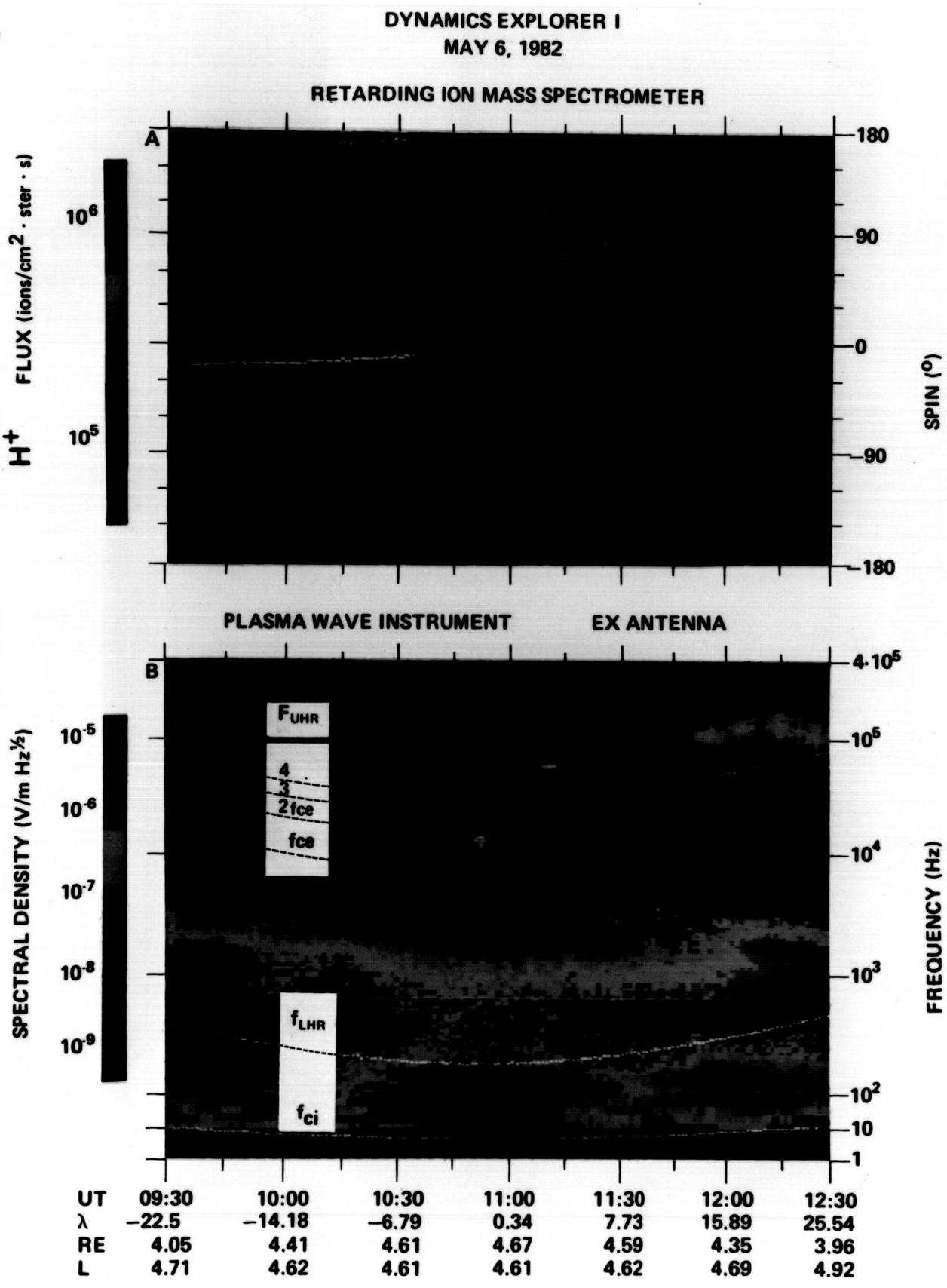
DYNAMICS EXPLORER I
MAY 6, 1982
RETARDING ION MASS SPECTROMETER
A
H+
FLUX (ions/cm2 · ster · s)
10^6
10^5
180
90
0
-90
-180
SPIN (°)
PLASMA WAVE INSTRUMENT
EX ANTENNA
B
SPECTRAL DENSITY (V/m Hz½)
10^-5
10^-6
10^-7
10^-8
10^-9
F_UHR
4
3
2fce
fce
f_LHR
f_ci
4·10^5
10^5
10^4
10^3
10^2
10
1
FREQUENCY (Hz)
UT 09:30 10:00 10:30 11:00 11:30 12:00 12:30
λ -22.5 -14.18 -6.79 0.34 7.73 15.89 25.54
RE 4.05 4.41 4.61 4.67 4.59 4.35 3.96
L 4.71 4.62 4.61 4.61 4.62 4.69 4.92
DAY 126

Plate 7

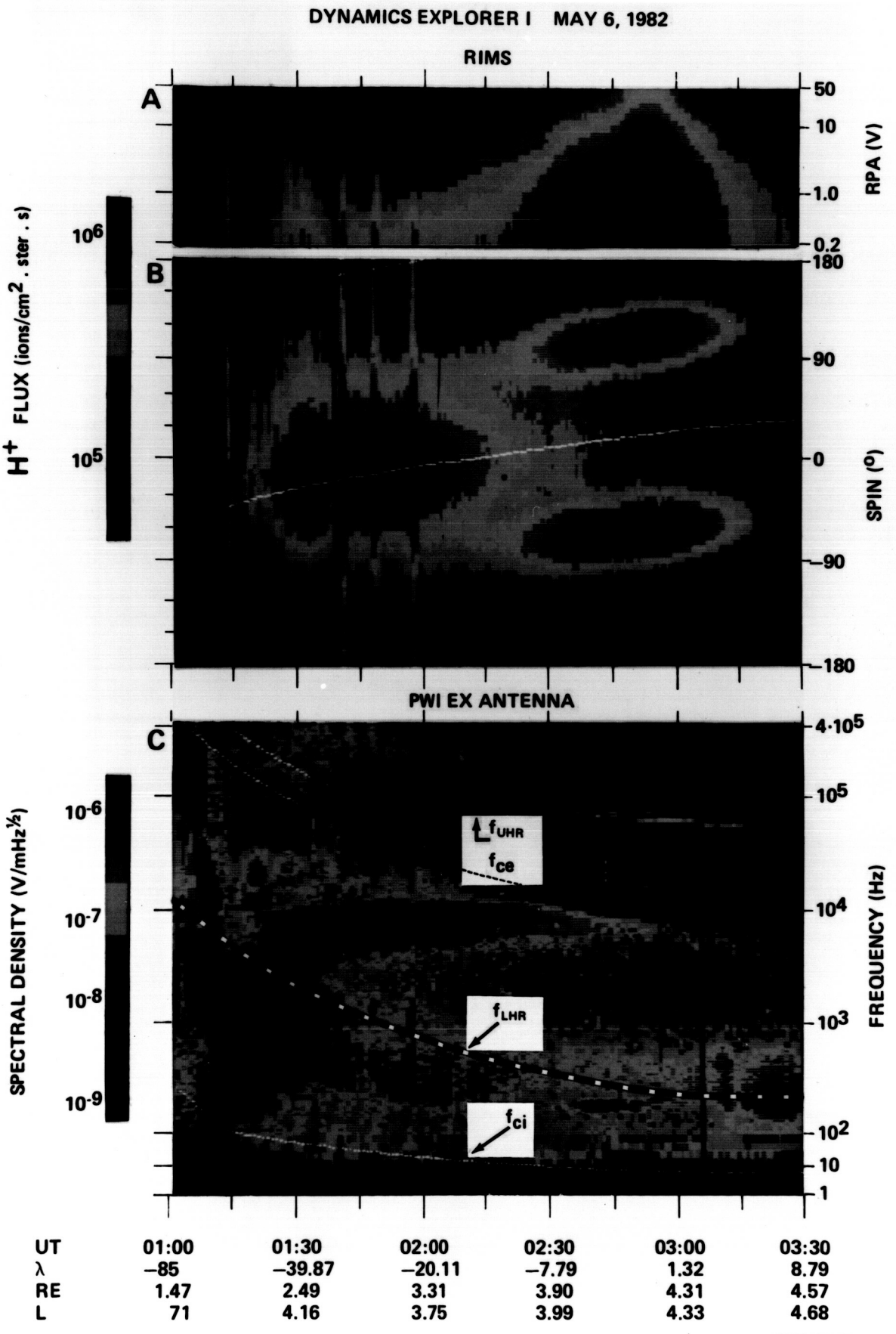
DYNAMICS EXPLORER I MAY 6, 1982
RIMS
A
B
50
10
1.0
0.2
RPA (V)
10^6
10^5
H^+ FLUX (ions/cm^2 . ster . s)
180
90
0
−90
−180
SPIN (°)
PWI EX ANTENNA
C
$4\cdot10^5$
10^5
10^4
10^3
10^2
10
1
FREQUENCY (Hz)
10^{-6}
10^{-7}
10^{-8}
10^{-9}
SPECTRAL DENSITY (V/mHz$^{1/2}$)
f_{UHR}
f_{ce}
f_{LHR}
f_{ci}
UT 01:00 01:30 02:00 02:30 03:00 03:30
λ −85 −39.87 −20.11 −7.79 1.32 8.79
RE 1.47 2.49 3.31 3.90 4.31 4.57
L 71 4.16 3.75 3.99 4.33 4.68
DAY 126

Plate 8

DYNAMICS EXPLORER I
MARCH 27, 1982

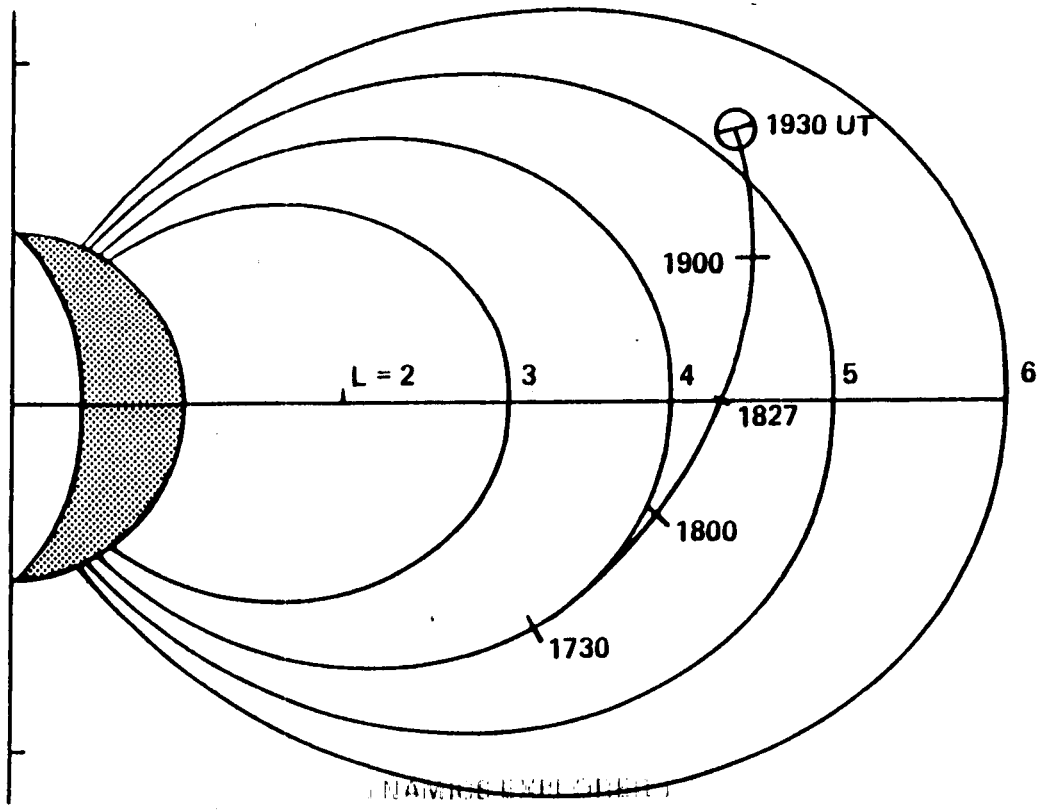

DAY 86

DYNAMICS EXPLORER I

MARCH 27, 1982

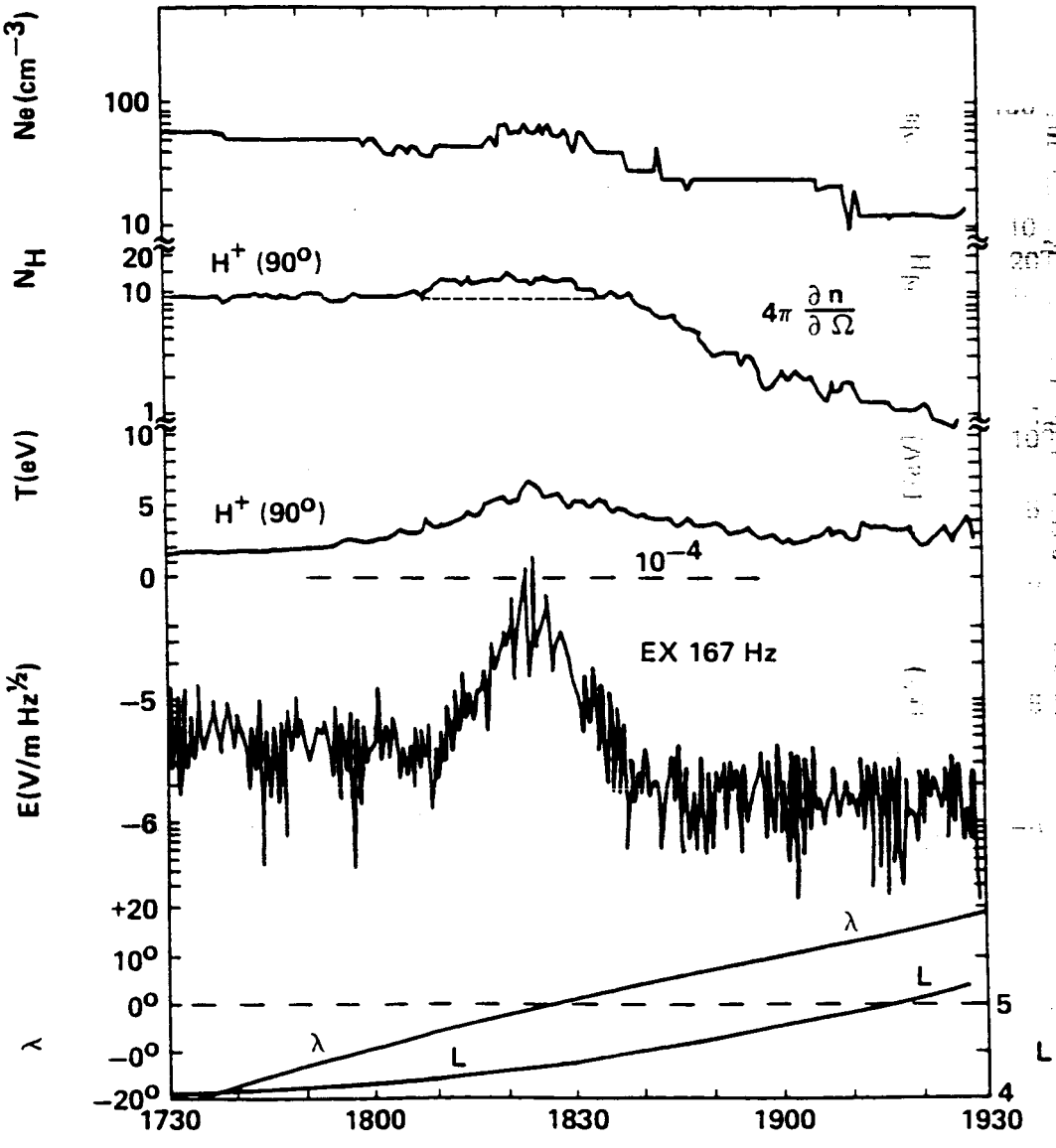

FIGURE 2

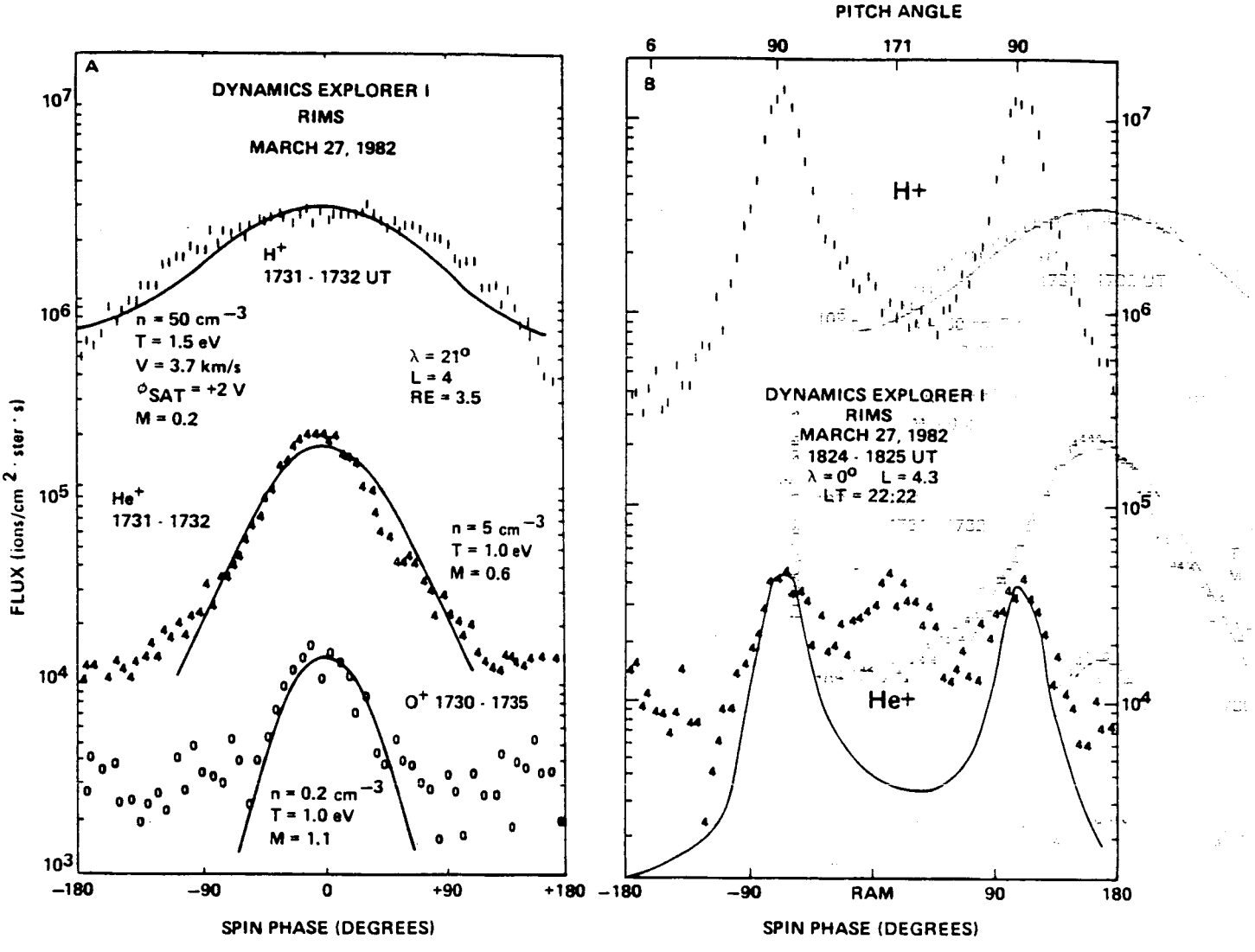
A
DYNAMICS EXPLORER I
RIMS
MARCH 27, 1982
H+
1731 - 1732 UT
n = 50 cm−3
T = 1.5 eV
V = 3.7 km/s
ϕSAT = +2 V
M = 0.2
λ = 21°
L = 4
RE = 3.5
He+
1731 - 1732
n = 5 cm−3
T = 1.0 eV
M = 0.6
O+ 1730 - 1735
n = 0.2 cm−3
T = 1.0 eV
M = 1.1
FLUX (ions/cm2 · ster · s)
SPIN PHASE (DEGREES)
PITCH ANGLE
6
90
171
90
B
H+
DYNAMICS EXPLORER I
RIMS
MARCH 27, 1982
1824 - 1825 UT
λ = 0° L = 4.3
LT = 22:22
He+
RAM
SPIN PHASE (DEGREES)

FIGURE 3

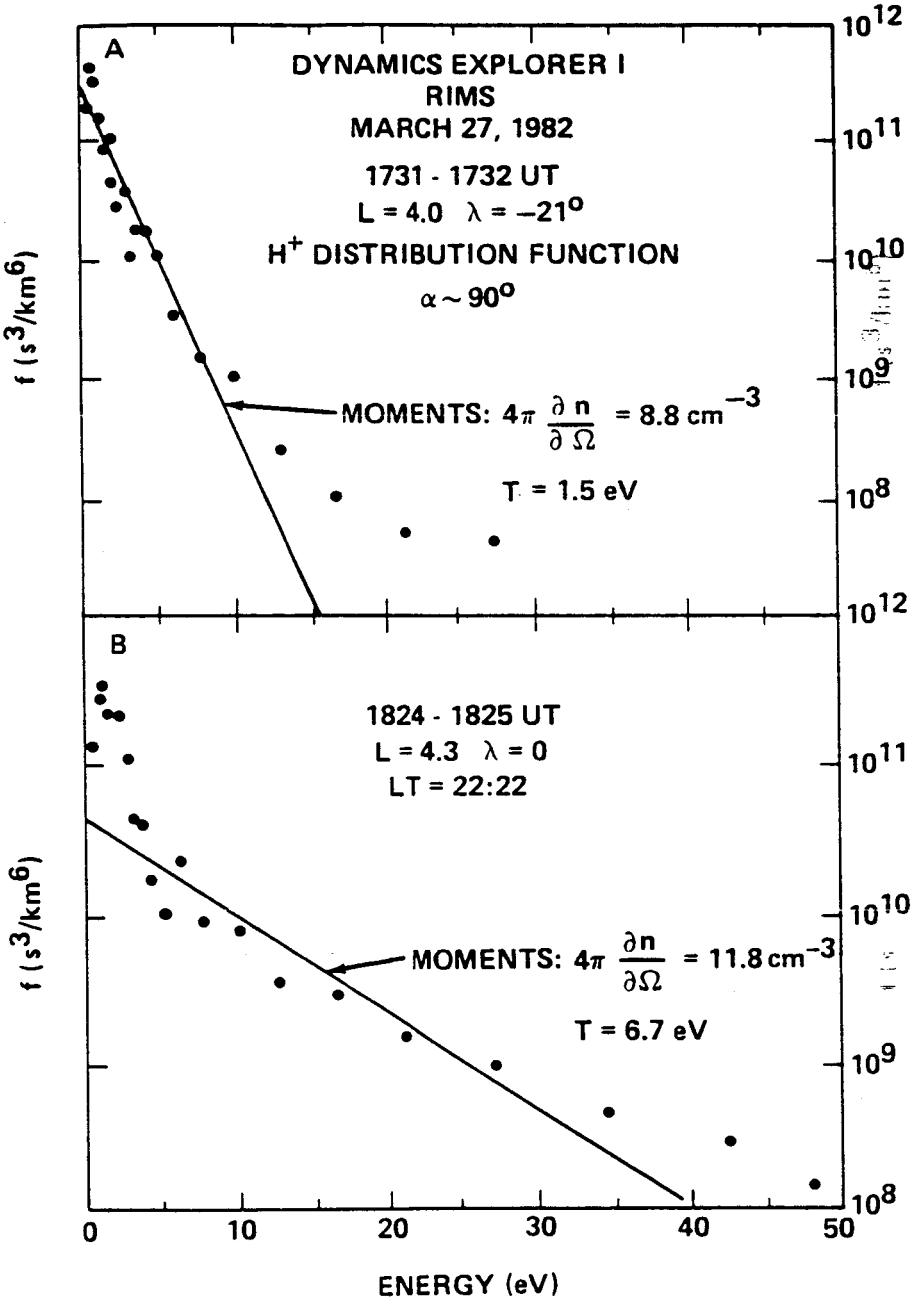
A
DYNAMICS EXPLORER I
RIMS
MARCH 27, 1982
1731 - 1732 UT
L = 4.0 λ = −21°
H+ DISTRIBUTION FUNCTION
α ~ 90°
MOMENTS: 4π ∂n/∂Ω = 8.8 cm−3
T = 1.5 eV
B
1824 - 1825 UT
L = 4.3 λ = 0
LT = 22:22
MOMENTS: 4π ∂n/∂Ω = 11.8 cm−3
T = 6.7 eV
f (s3/km6)
f (s3/km6)
10^12
10^11
10^10
10^9
10^8
0
10
20
30
40
50
ENERGY (eV)

FIGURE 4

DYNAMICS EXPLORER
MARCH 27, 1982
1822 - 1828 UT

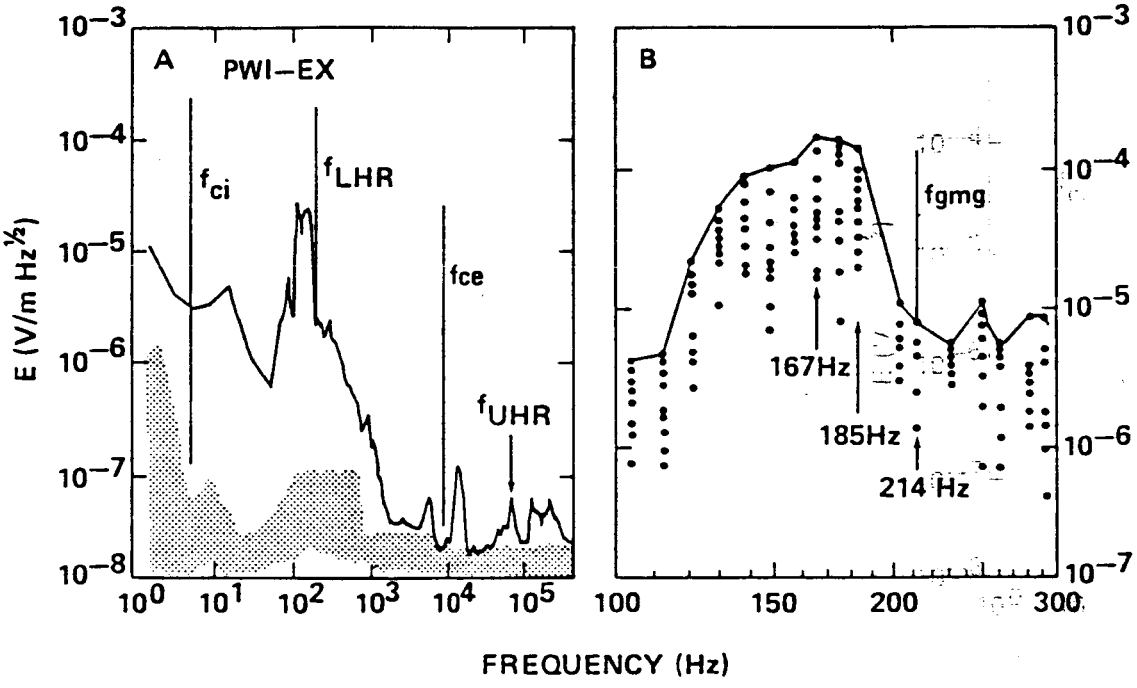

FIGURE 5

DYNAMICS EXPLORER I
FEBRUARY 21, 1982

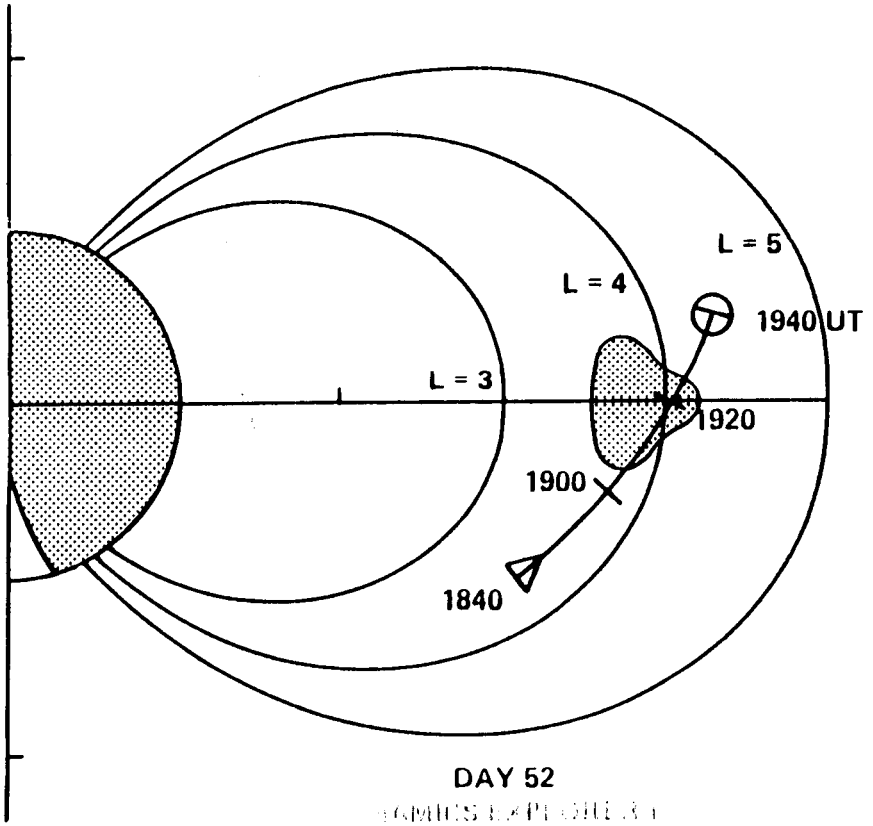

DAY 52

where is the plasmapause? check later data

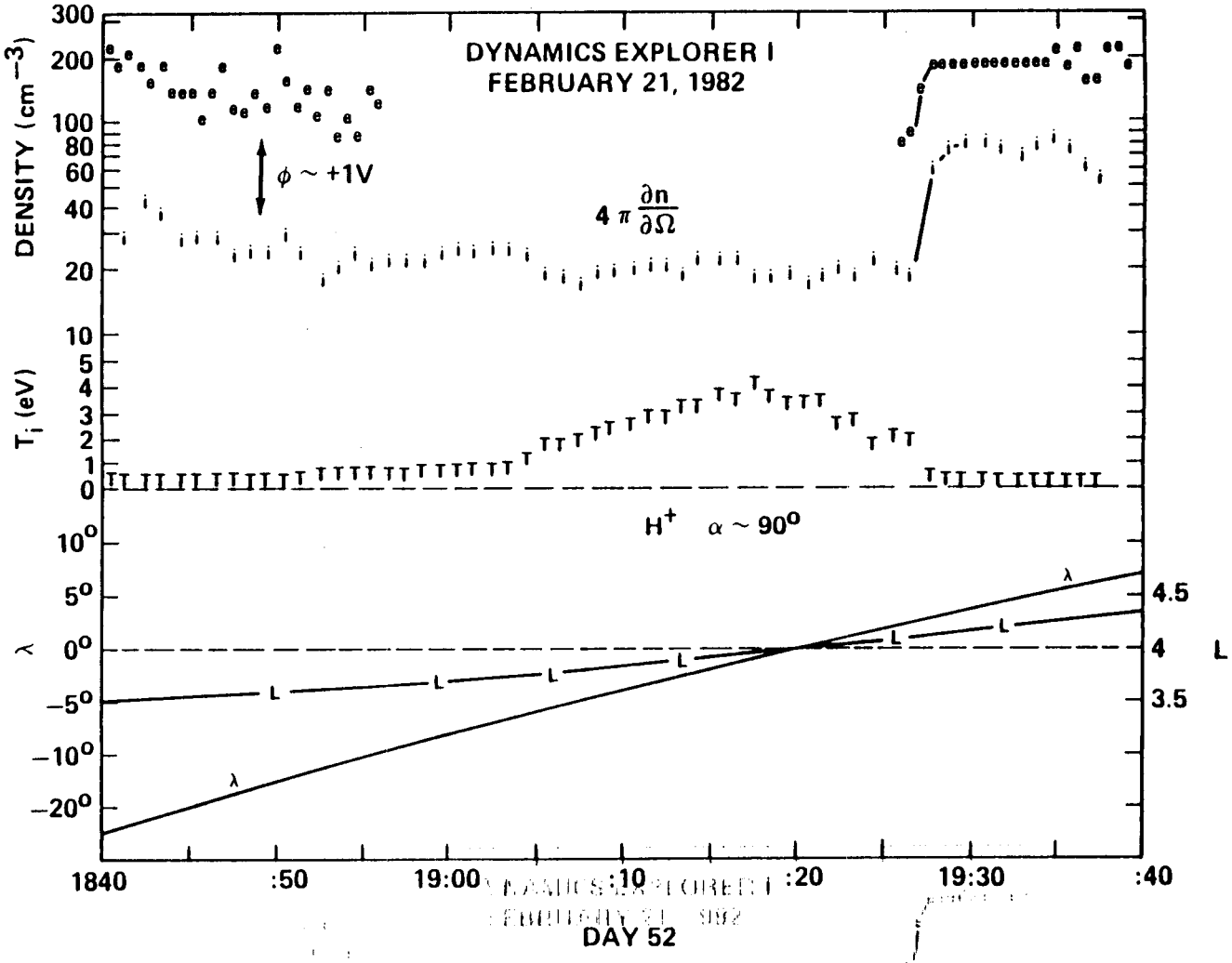
DYNAMICS EXPLORER I
FEBRUARY 21, 1982
DENSITY (cm^{-3})
300
200
100
80
60
40
20
$\phi \sim +1V$
$4\pi \frac{\partial n}{\partial \Omega}$
T_i (eV)
10
5
4
3
2
1
0
H^+ $\alpha \sim 90^o$
10^o
5^o
0^o
-5^o
-10^o
-20^o
λ
L
4.5
4
3.5
L
1840
:50
19:00
:10
:20
19:30
:40
DAY 52

FIGURE 7

DE–1 RIMS
FEBRUARY 21, 1982

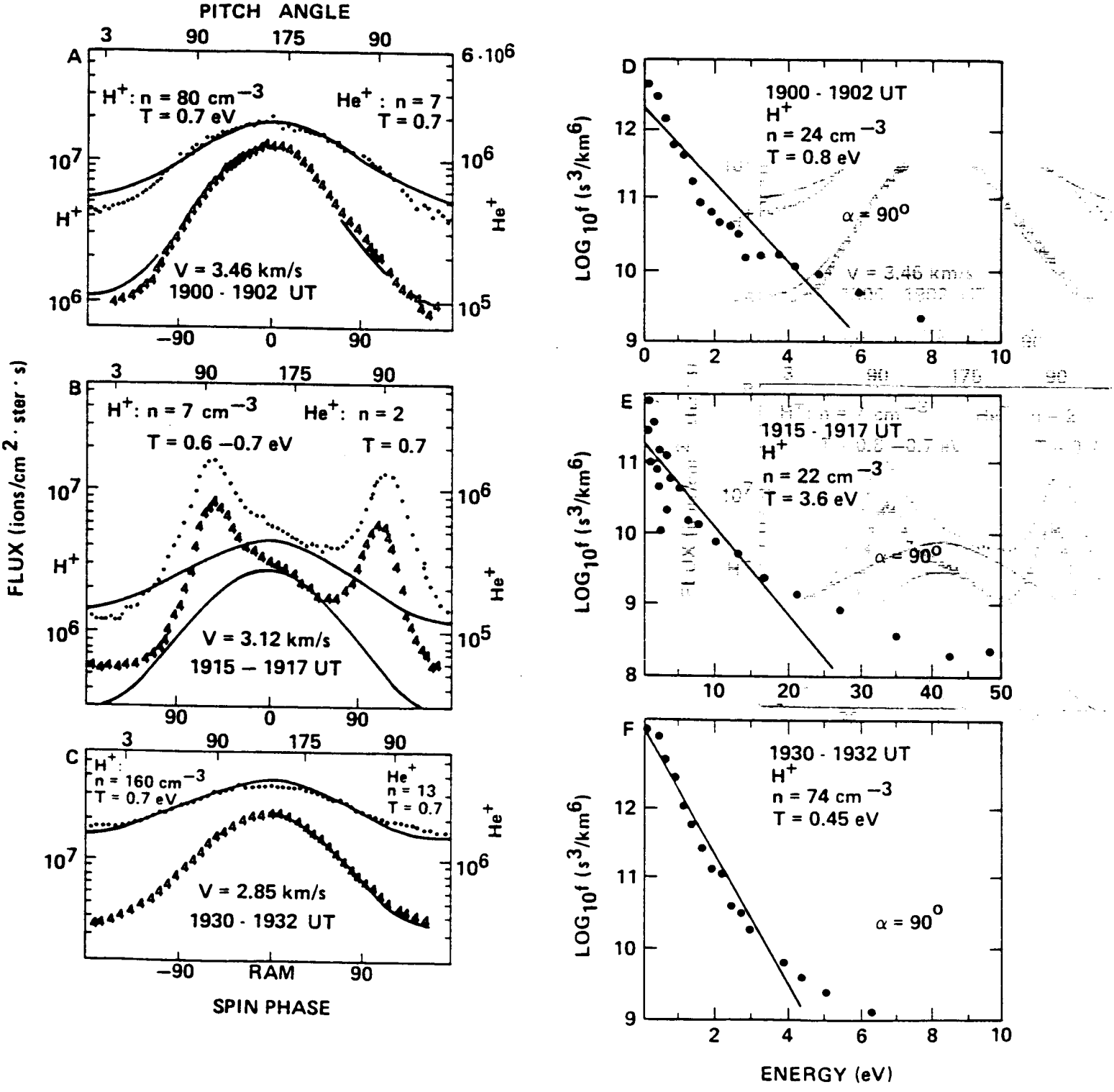

FIGURE 8

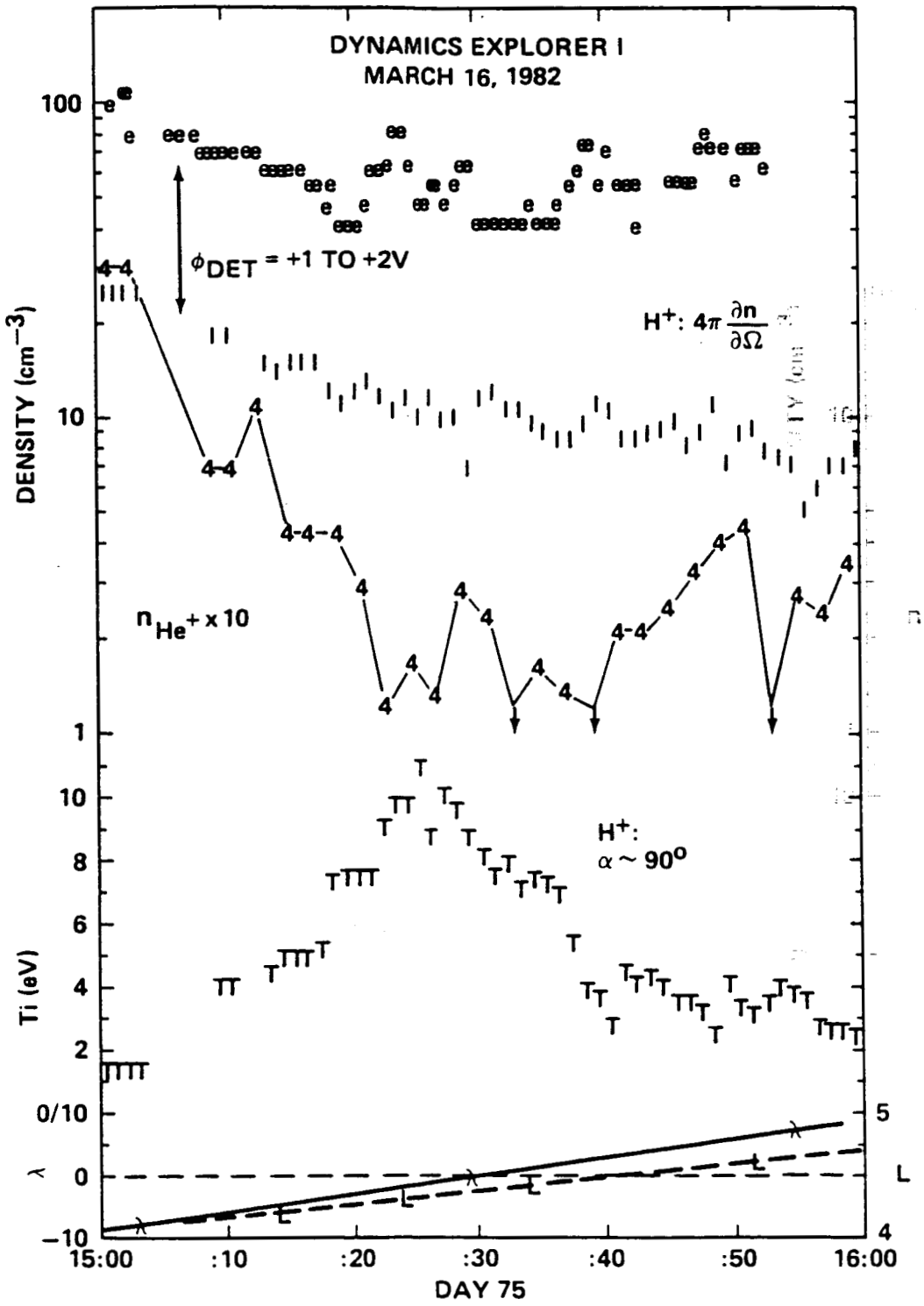
DYNAMICS EXPLORER I
MARCH 16, 1982
DENSITY (cm^{-3})
100
10
1
ϕ_{DET} = +1 TO +2V
H^+: $4\pi \frac{\partial n}{\partial \Omega}$
$n_{He^+} \times 10$
H^+:
$\alpha \sim 90^o$
Ti (eV)
10
8
6
4
2
0/10
0
−10
λ
5
L
4
15:00
:10
:20
:30
:40
:50
16:00
DAY 75

FIGURE 9

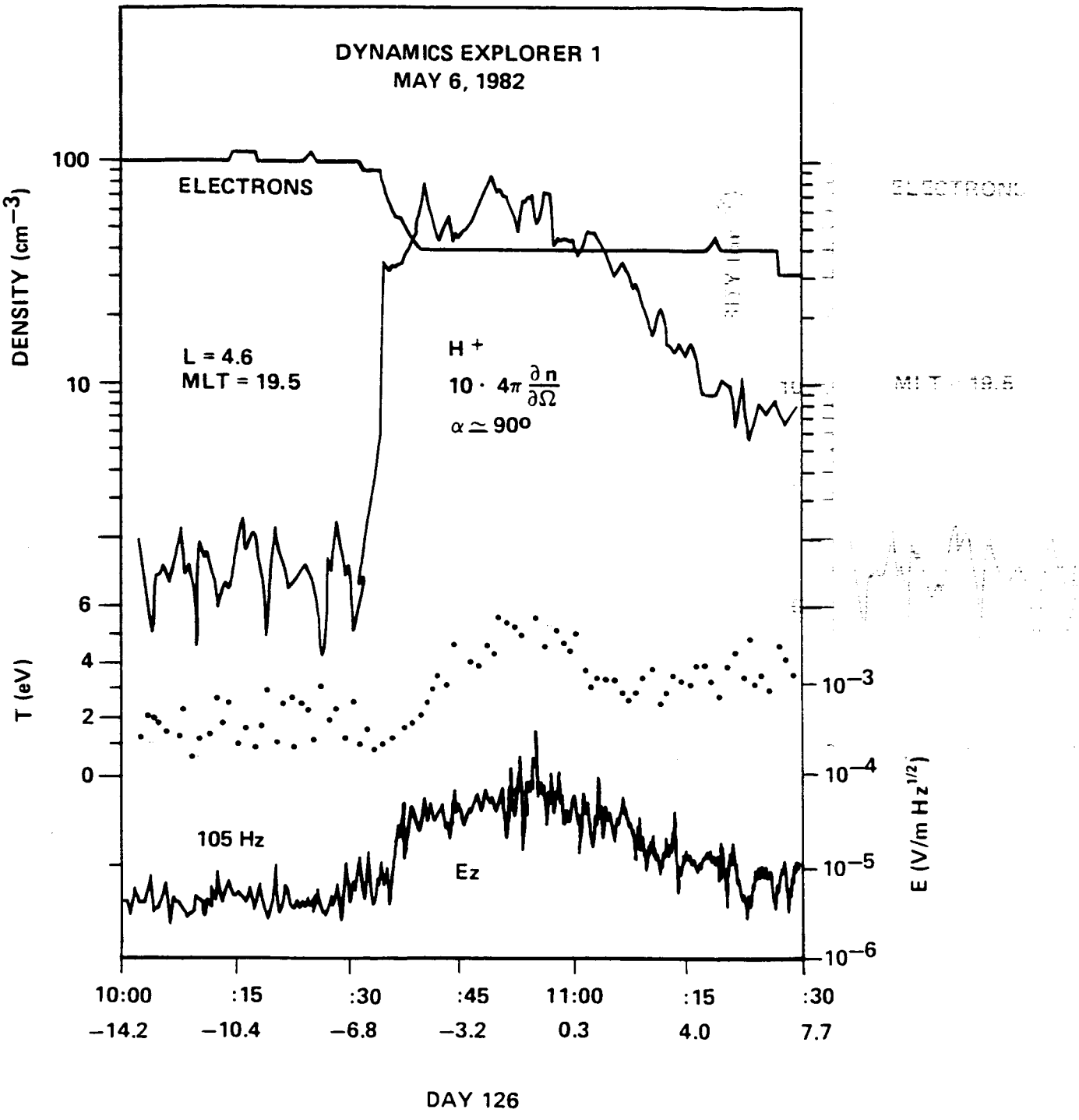
DYNAMICS EXPLORER 1
MAY 6, 1982
DENSITY (cm^{-3})
100
10
ELECTRONS
L = 4.6
MLT = 19.5
H +
10 · 4π ∂n/∂Ω
α ≃ 90°
T (eV)
6
4
2
0
105 Hz
Ez
10^{-3}
10^{-4}
10^{-5}
10^{-6}
E (V/m Hz$^{1/2}$)
10:00
:15
:30
:45
11:00
:15
:30
−14.2
−10.4
−6.8
−3.2
0.3
4.0
7.7
DAY 126

Figure 10

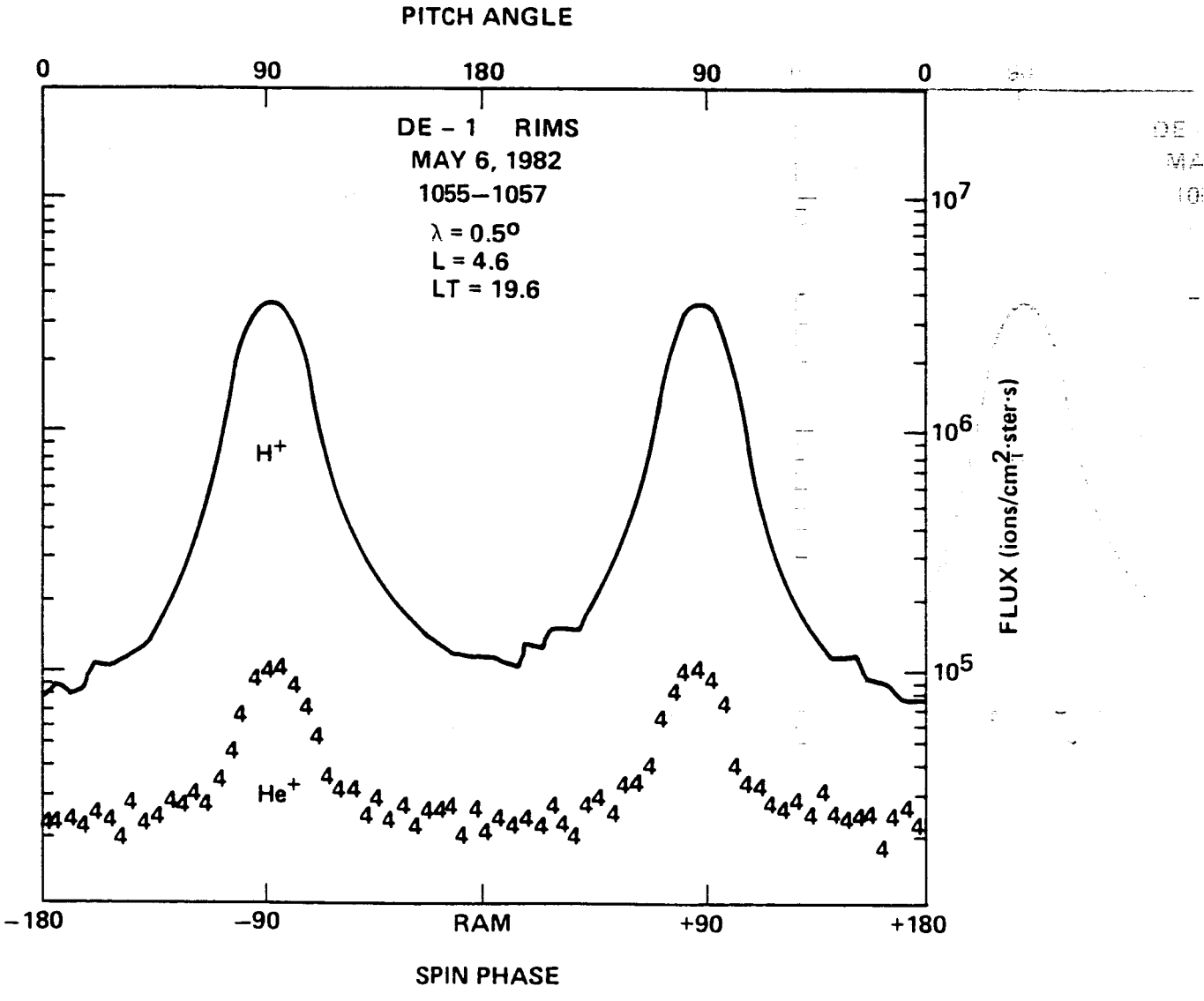
PITCH ANGLE
0
90
180
90
0
DE – 1 RIMS
MAY 6, 1982
1055–1057
λ = 0.5°
L = 4.6
LT = 19.6
10^7
10^6
10^5
FLUX (ions/cm^2·ster·s)
H$^+$
He$^+$
–180
–90
RAM
+90
+180
SPIN PHASE

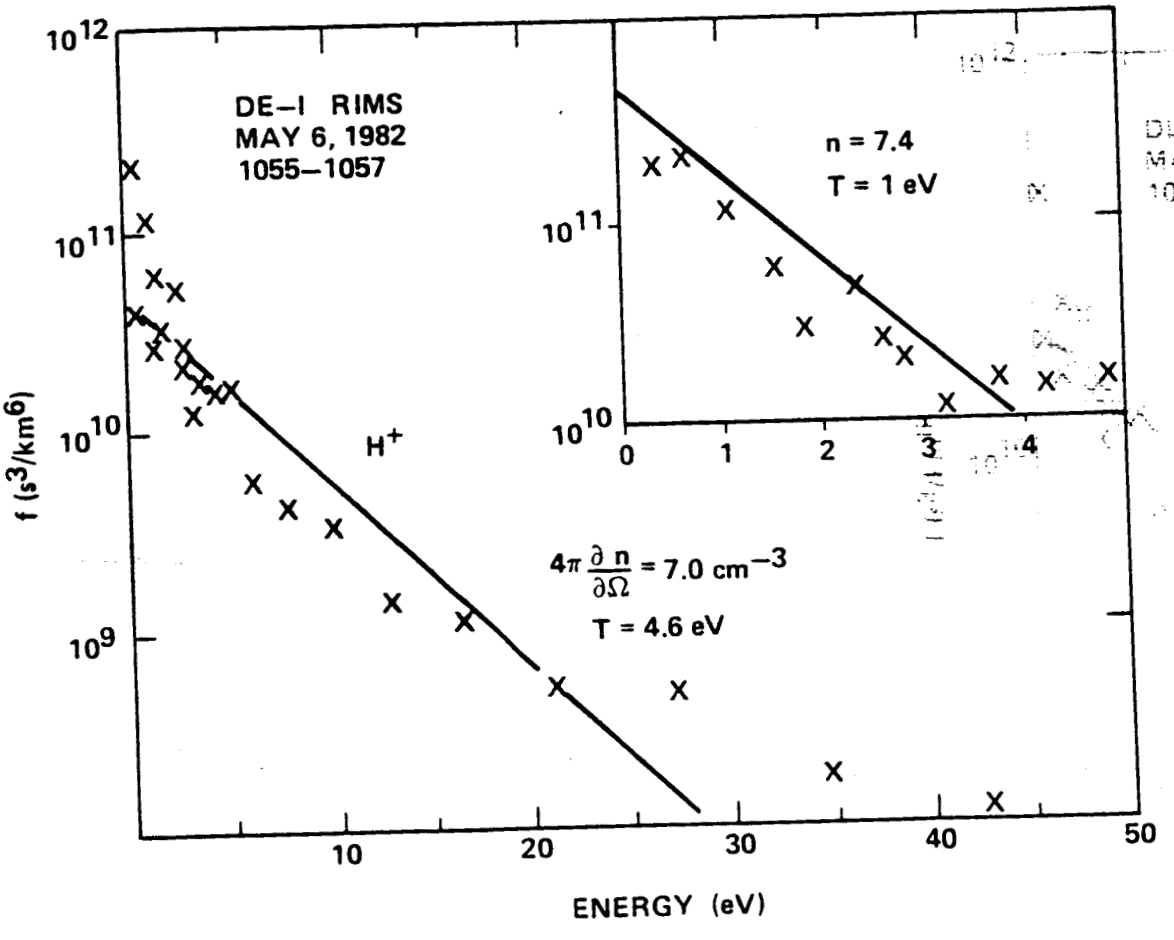
DE–I RIMS
MAY 6, 1982
1055–1057
10^{12}
10^{11}
10^{10}
10^{9}
f (s^3/km^6)
H^+
$4\pi \frac{\partial n}{\partial \Omega} = 7.0\ cm^{-3}$
T = 4.6 eV
n = 7.4
T = 1 eV
0
1
2
3
4
10
20
30
40
50
ENERGY (eV)

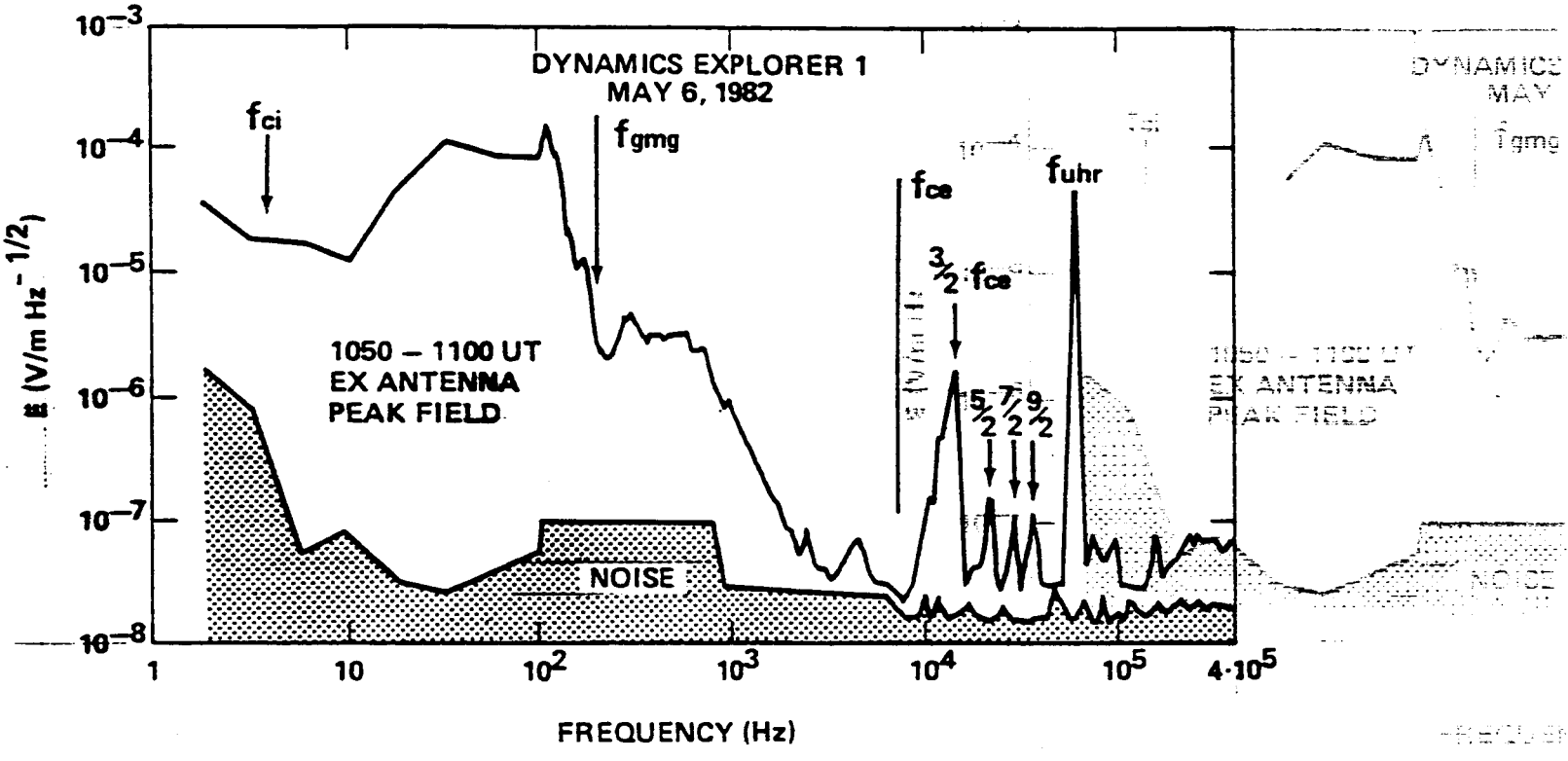
DYNAMICS EXPLORER 1
MAY 6, 1982
fci
fgmg
fce
fuhr
3/2 fce
5/2 fce
7/2 fce
9/2 fce
1050 – 1100 UT
EX ANTENNA
PEAK FIELD
NOISE
E (V/m Hz^-1/2)
10^-3
10^-4
10^-5
10^-6
10^-7
10^-8
1
10
10^2
10^3
10^4
10^5
4·10^5
FREQUENCY (Hz)

FIGURE 13

DE–1 AND ISEE–1
MAY 6, 1982

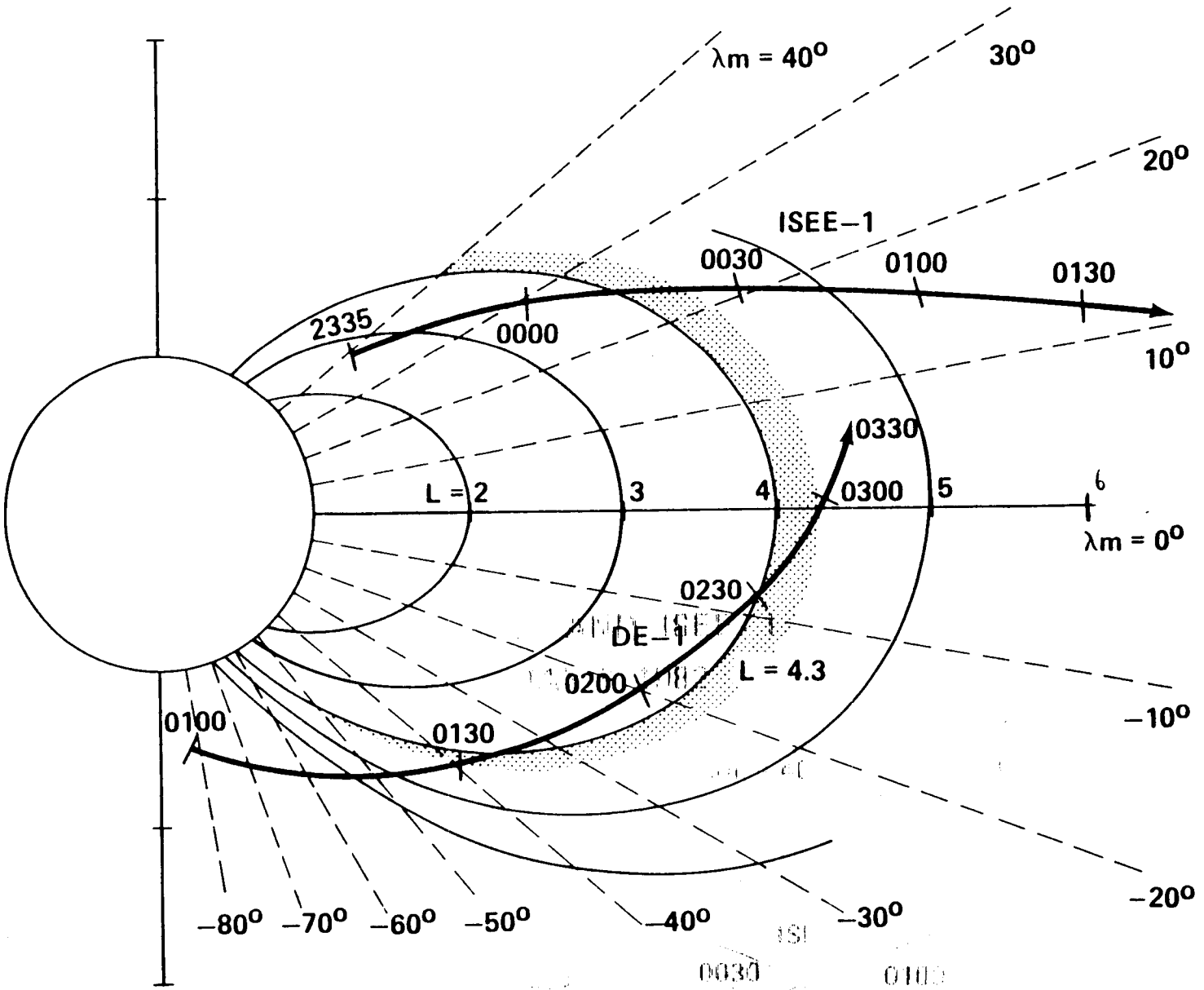

DAY 126

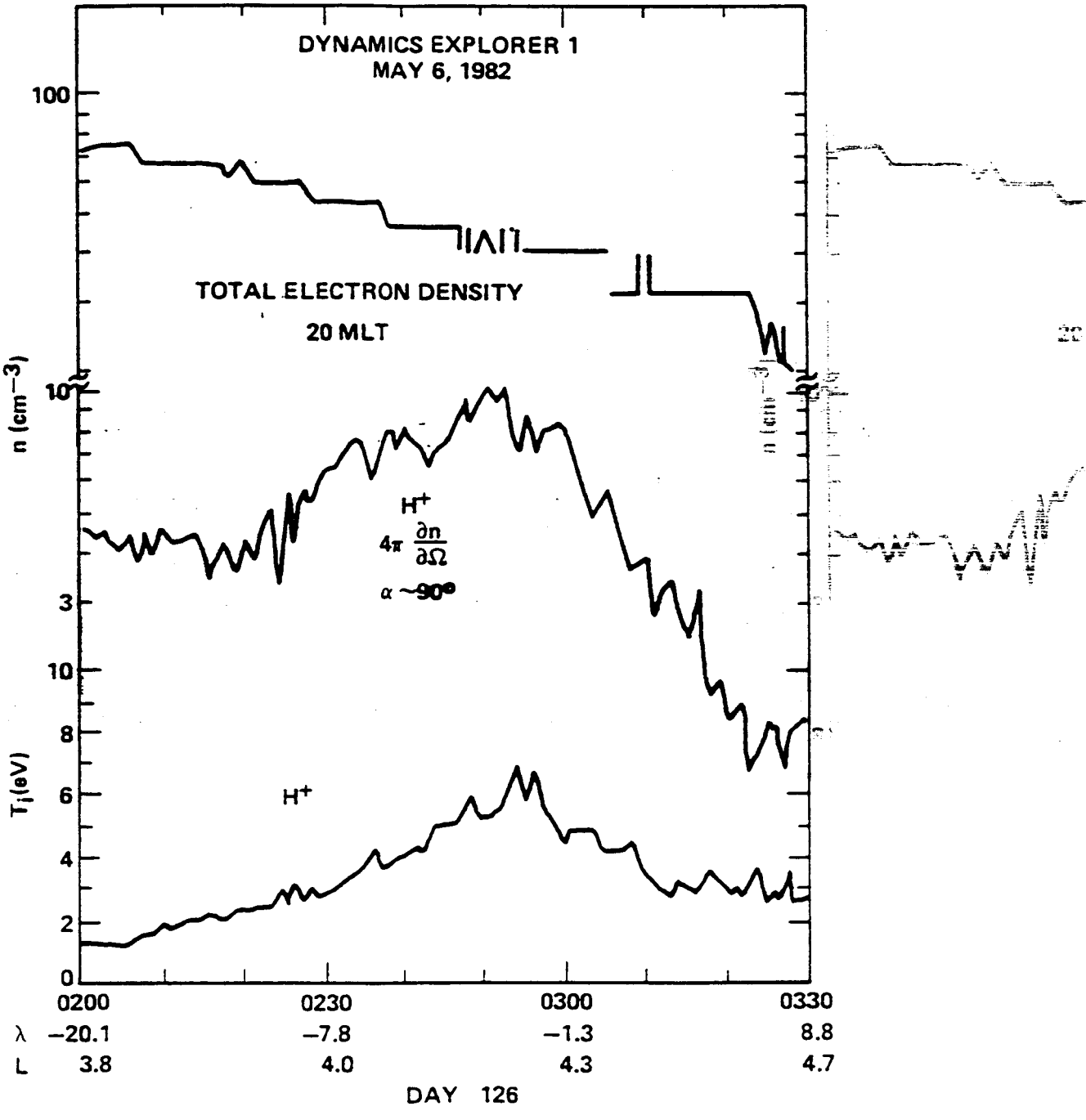
DYNAMICS EXPLORER 1
MAY 6, 1982
TOTAL ELECTRON DENSITY
20 MLT
n (cm⁻³)
100
10
3
H+
4π ∂n/∂Ω
α ~90°
10
8
6
4
2
0
Ti(eV)
H+
0200
0230
0300
0330
λ −20.1
−7.8
−1.3
8.8
L 3.8
4.0
4.3
4.7
DAY 126

FIGURE 15

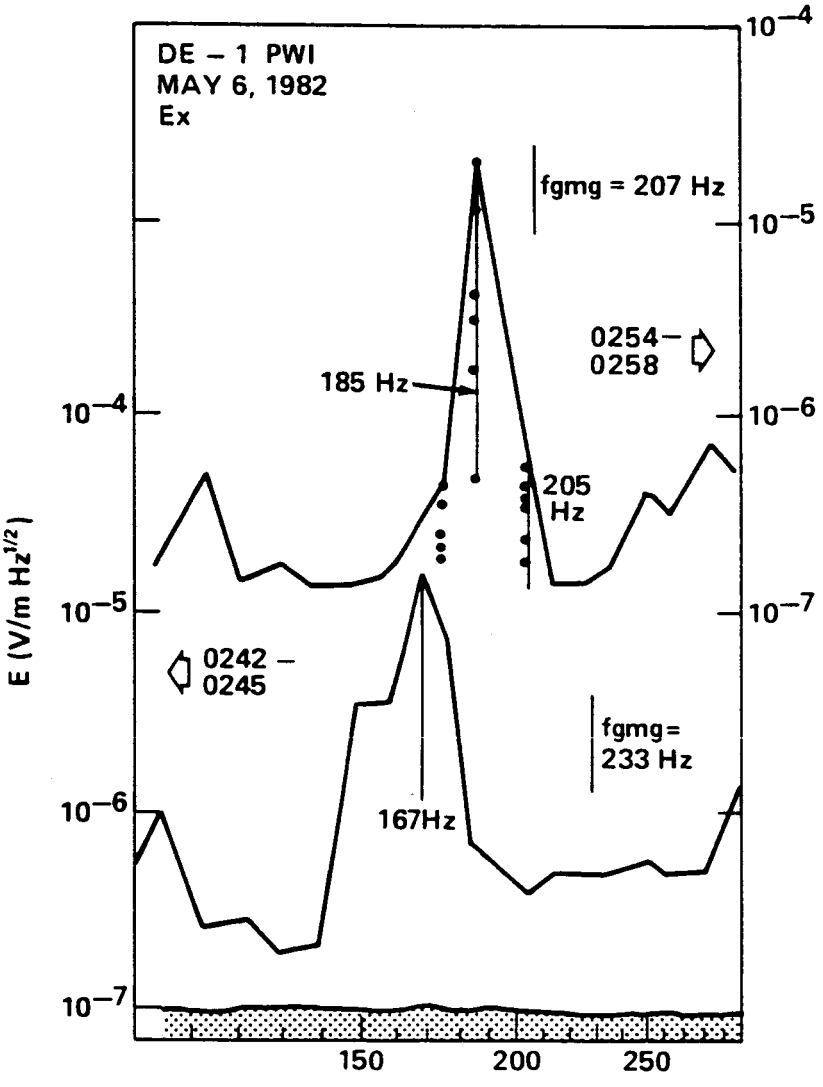
DE – 1 PWI
MAY 6, 1982
Ex
fgmg = 207 Hz
0254 –
0258
185 Hz
205
Hz
0242 –
0245
fgmg=
233 Hz
167Hz
E (V/m Hz$^{1/2}$)
10^{-4}
10^{-5}
10^{-6}
10^{-7}
150
200
250

Figure 16

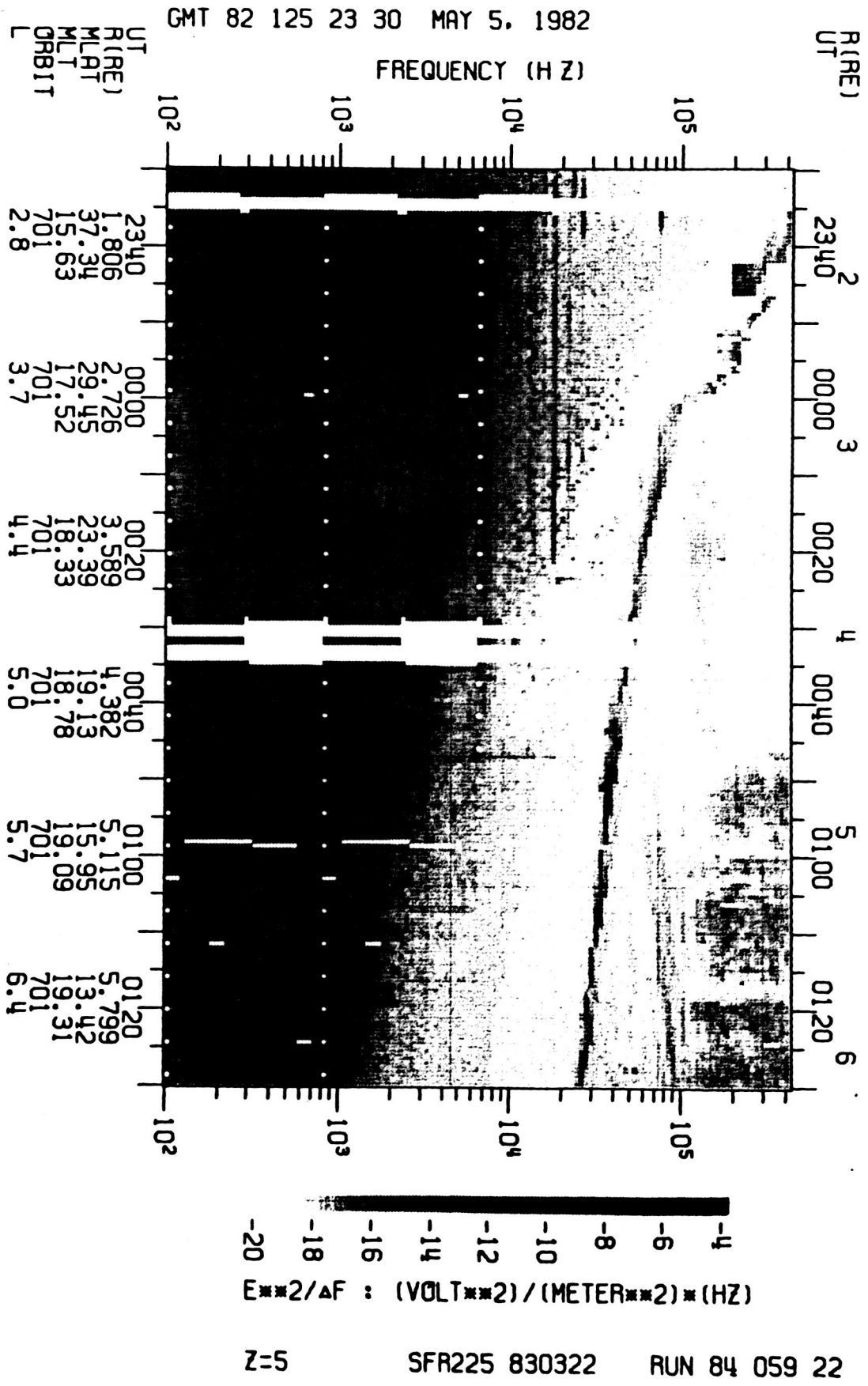
GMT 82 125 23 30 MAY 5, 1982
FREQUENCY (HZ)
UT R(RE) MLAT MLT ORBIT L
R(RE) UT
2340 0000 0020 0040 0100 0120
2 3 4 5 6
E**2/ΔF : (VOLT**2)/(METER**2)*(HZ)
Z=5
SFR225 830322
RUN 84 059 22

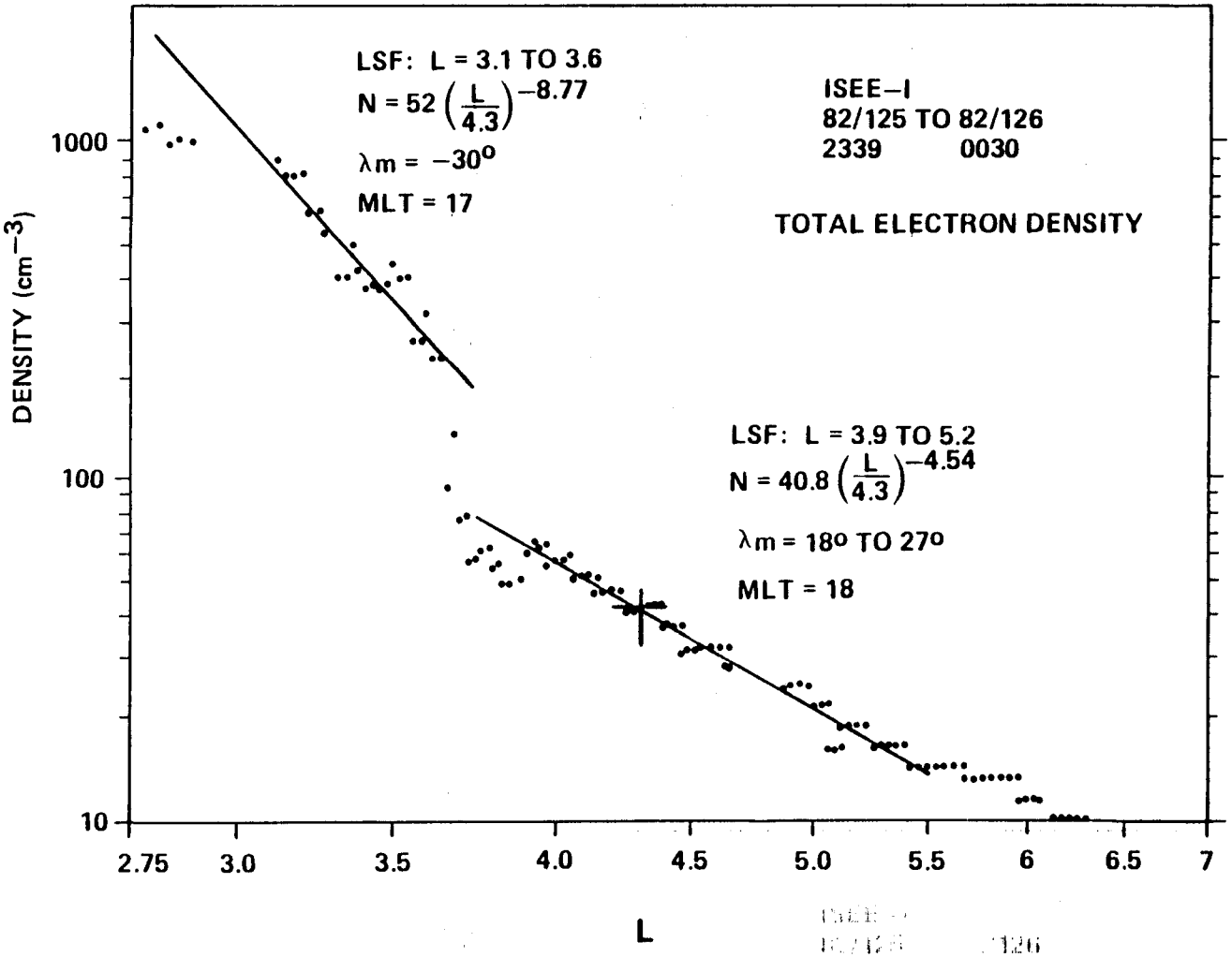
LSF: L = 3.1 TO 3.6
N = 52 (L/4.3)^−8.77
λm = −30°
MLT = 17
ISEE–I
82/125 TO 82/126
2339 0030
TOTAL ELECTRON DENSITY
LSF: L = 3.9 TO 5.2
N = 40.8 (L/4.3)^−4.54
λm = 18° TO 27°
MLT = 18
DENSITY (cm^−3)
1000
100
10
2.75
3.0
3.5
4.0
4.5
5.0
5.5
6
6.5
7
L

FIGURE 18

A MAGNETOSPHERIC TANDEM MIRROR

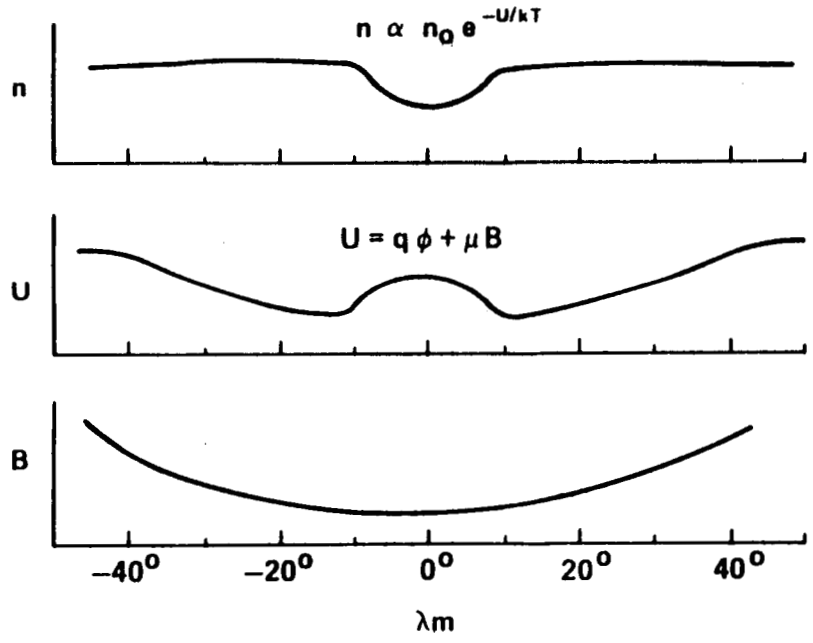

PLASMA HEATING AT THE EARTH'S MAGNETIC EQUATOR